ADDIS ABABA UNIVERSITY

ADDIS ABABA INSTITUTE OF TECHNOLOGY

SCHOOL OF CIVIL AND ENVIRONMENTAL ENGINEERING

EXPERIMENTAL INVESTIGATION ON THE BOND PERFORMANCE OF STEEL TO OUTER CONCRETE INTERFACES IN CONCRETE-ENCASED CONCRETE-FILLED STEEL TUBE

A Thesis in STRUCTURAL ENGINEERING

By Muluken Bogale

Submission Date: 6/11/2013

Addis Ababa

A Thesis

Submitted in Partial Fulfillment of the Requirements for the Degree of Master of Science

The undersigned have examined the thesis entitled '**Experimental Investigation on The Bond Performance of Steel to outer Concrete Interfaces in Concrete-Encased Concrete-Filled Steel Tube**' a candidate for the degree of **Master of Science** and hereby certify that it is worthy of acceptance.

Prof. Girma Zerayouhannes		
Advisor	Signature	Date
Dr.-Ing Adil Zekaria		
Internal Examiner	Signature	Date
Dr. Abrham Gebre		
External Examiner	Signature	Date
Chair person	Signature	Date

UNDERTAKING

I certify that research work titled "**Experimental Investigation on The Bond Performance of Steel to outer Concrete Interfaces in Concrete-Encased Concrete-Filled Steel Tube**" is my own work. The work has not been presented elsewhere for assessment. Where material has been used from other sources it has been properly acknowledged / referred.

Muluken Bogale

.

ABSTRACT

Composite structure in the high-rise building, industrial workshop, and bridge subjected to loading, which the steel element independently exposed to loading and resulted in the occurrence of slip between steel and concrete, which reduces the carrying capacity. The bond performance steel-concrete interfaces are essential for the proper function of a composite structure. This paper studies the bond performance of outer concrete and steel interfaces of concrete-encased concrete-filled steel tubes.

A series of push-out tests on nine CECFST specimens are conducted with the parameter of concrete compressive strength, concrete cover, and spacing of transverse reinforcement. The average bond stress to slip relationship and strain distribution in outer concrete along the longitudinal height direction were cautiously investigated. It was found that the bond stress to slip curve has four regions; linear region, non-linear region, post-peak softening region, and residual region. The shear resistance on the four regions comes from chemical adhesion, steel surface roughness, and steel tube irregularity. The average bond strength of outer RC to CFST interfaces was 1.78N/mm^2, while the minimum and maximum bond strength were 1.18N/mm^2 and 2.3N/mm^2, respectively, which provided for stress limit in FEM.

The influence of various parameters was recorded, analyzed, and discussed. In general, the test result indicates that the bond strength increases with the increase of concrete compressive strength. Concrete cover has a moderate effect on the bond performance, and spacing of transverse reinforcement has a minor effect. Finally, a comparison is made between the experimental result of bond stress to slip curves and a finite element modeling, a good result achieved.

Keywords: Concrete-Encased Concrete-Filled Steel Tube; Pushout Test; Bond Stress; Finite Element Model and Slip

ACKNOWLEDGEMENT

Throughout the writing of this research, I have received a great deal of support and assistance. I would first like to thank my advisor professor Girma Zerayouhannes for the patience and support.

I also like to thank Dr. Esayas G/youhannes and Dr. Abrham Gebre for the valuable guidance constructive comments, and useful suggestions.

I also like to express my deepest gratitude to Biniyam, Fikeru. B and Webet.A for assisting me in the construction material test.

My warm heartfelt thanks go to Hamelmal Shibeshi whose support was unquestioned. Without her, this research would have been truly challenging.

Likewise, thank you to my parents Bogale Admasu and Tobiyaw Lema. In addition, I would like to offer sincerely to Mesfin Bogale, Paulos Bogale, Mengistu Admassu, Demekech Begashaw, Binyam Kidane, Addisu Mengistu, Netsanet Mengistu for your endless support and sympathetic ear. You always had faith in me, and I respect that.

TABLE OF CONTENTS

LIST OF SYMBOLS

RC	Reinforced Concrete
CFST	Concrete-Filled Steel Tube
CE-CFST	Concrete-Encased Concrete-Filled Steel Tube
FEA	Finite Element Analysis
f_y	Yield Strength of Steel
f_u	Ultimate Strength of Steel
E_s	Elastic Modulus of Steel
E_{cm}	Elastic Modulus of Concrete
ν	Poison Ratio
f_{ck}	Characteristic Cylinder Compressive Strength of Concrete
t	Thickness of Steel Tube
D	Diameter of Steel Tubes
N_{ue}	Ultimate Push Load
τ_u	Ultimate Bond Stress
S	Slip at The Interfaces
ε	strain
CFDST	Concrete Filled Double Skin Steel Tube

LIST OF TABLES

LIST OF FIGURES

CHAPTER 1 INTRODUCTION

1.1 General background

Concrete-encased concrete-filled steel tube (CE-CFST) is a special type of composite member, which consists of inner concrete filled steel tube and outer reinforced concrete member, which has been used in high rise building, factories, power station, industrial workshops, and long-span bridges. It has a better structural performance like high bearing capacity, ductility, small cross-sectional size, and seismic resistance than conventional reinforced concrete column due to the existence of concrete-encased steel and has better fire resistance and durability under corrosive environment than that of concrete-filled steel tube, because of the confinement of outer reinforced concrete component. The longitudinal bar in the reinforced concrete beam can pass through the encased concrete CFST and anchored to outer reinforced concrete of concrete-encased CFST, which have an easier connection to RC beams shown in Fig 1.1.

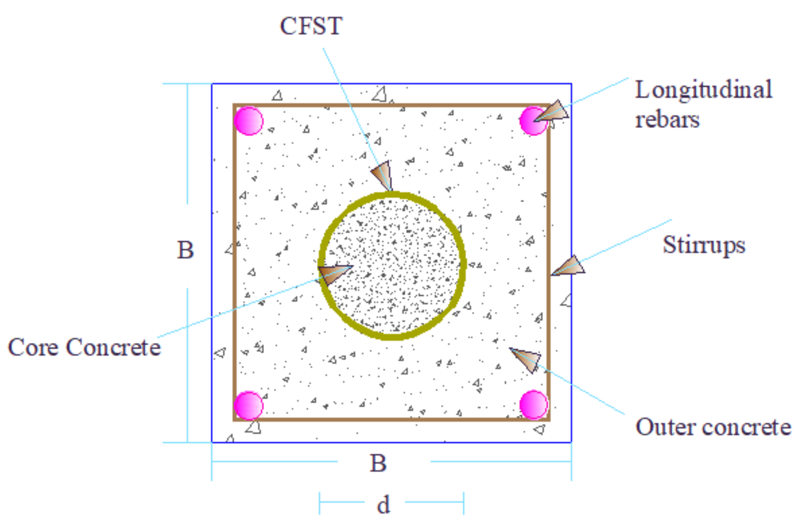

Fig 1. 1 Typical Concrete-Encased CFST.

The interaction between the steel tube and concrete affects the stress transfer of composite action. But slip can occur between steel tube and outer concrete due to geometric discontinuity at connections, foundations support, load introduction areas, and location with the change of cross-sections. This condition disturbs natural composite action by reducing the load transfer from steel to outer reinforced concrete and steel tube to core concrete. Therefore, the natural composite interaction between concrete and steel in composite structures is necessary to guarantee the higher performance of steel-concrete composite structures.

There are two steel-concrete interfaces in Concrete-encased concrete-filled steel tube members, those are the interfaces between core concrete and steel tube and the interfaces between outer concrete and steel tube. The interaction between the two interfaces is significant for the transmission of load in composite action. However, researchers used the same bond strength for both interfaces. Due to different deformation trend and confinement effect, the core and outer concrete during shrinkage and under loading is different. So that, the investigation of bond performance between the steel tube and outer RC is crucial for understanding the carrying capacity of CE-CFST.

Considering the above discussion, this paper presents a test program to investigate the bond performance between the outer concrete and outer surface of steel tubes. The influence of different parameters such as restriction of concrete encasement, concrete strength, and lateral confinement on the bond performance is then discussed.

1.2 Significance of the research

Understanding the accurate carrying capacity of the composite is important for the safe design of structures. In some cases, the steel tube, independently exposed to axial load or bending. From that point onward, the applied load must be shared to outer concrete by bond stress. Otherwise, the capacity of the cross-section will vanish and resulted in a reduction in the design capacity of the cross-section. Design codes provide the minimum requirement of bond strength at the interfaces of the concrete-encased composite structure. If the prerequisite is not satisfied, the mechanical key or shear connectors are advised to be used. This study provides the bond strength of the CE-CFST at the interfaces between the outer concrete and outer steel tube surfaces for the design codes and for the designer.

1.3 Objective of the Study

General objectives

The main objective of this study is experimentally investigating the bond performance of steel-concrete interfaces in concrete-encased concrete-filled steel tube.

Specific Objectives

The specific objectives of this research are as follows:

- To conduct a series of pushout test on CE-CFST columns for steel tube to outer RC interfaces, exploring the mechanism of the load transfer on interfaces.
- To study influences of various parameters on the interface's behavior in CE-CFST such us concrete strength, concrete cover and spacing of transverse reinforcement.
- To study the behavior of average bond stress to slip curve.

1.4 Scope of the research

The research only focuses on the bond performance of steel tube to the outer concrete interface of concrete-encased concrete-filled steel tube and push-out test conducted for the experiment. No mechanical device or shear connector was used. Strain distribution on steel tube was not recorded.

1.5 Methodology

To meet the objectives of the thesis, works of literature are collected, and design codes are surveyed to evaluate the bond performance of composite structures at the interfaces: push-out test conducted for bond performance at the interfaces. Aside from dealing with the bond performance CE-CFST and modeling, the strain distribution, effect of an influential parameter, and load transfer to outer concrete were investigated. Finally, analytical modeling was used for the validation of the experimental result.

1.6 Thesis Organization

The thesis is organized into seven chapters. The study mainly focuses on the bond performance of steel to concrete interfaces in CE-CFST. The first chapter discusses the introduction of the study. Then various literature discussed the bond performance of the steel-concrete structure and composite structure in the second chapter. Furthermore, the load transfer mechanism from concrete to steel and the behavior of bond stress to slip curve are also presented. The experimental program was carried out in the third chapter. The fourth chapter was discussing the finite element analysis model for the pushout test. The experimental result on the behavior of bond stress to slip curve, strain distribution on outer concrete, and influence of various parameters were discussed in the fifth chapter. In chapter six, validation of the FEM was presented. The last chapter presents the conclusion and recommendation.

CHAPTER 2. LITERATURE REVIEW

2.1 General Background

Understanding of bond performance of steel-concrete interfaces in CECFST is important to know the capacity of the composite member. The review starts with explaining the behavior of concrete-encased concrete-filled steel tubes under axial compression, torsion, tension, and a combination of different loads. Then there was a brief description of the pushout test procedure and setup.

The review continued by summarizing the literature that was conducted on steel to the concrete interface of Concrete Filled Steel Tube, Steel Reinforced Concrete, and Concrete Encased Concrete Filled Steel Tube. Also included, different researcher recommendations to measure the bond strength of composite members and load transfer mechanism from steel to concrete.

Finally, the bond mechanism of steel concrete interfaces was described: when slip occurs between two materials, the first resistance comes from chemical adhesion. When the slip increases, the relative motion at the interfaces resisted by micro interlocking or steel surface roughness. Macro interlocking or steel tube irregularity contributes to the residual bond strength of the composite member.

2.2 Behavior of Concrete Encased Concrete Filled Steel Tube Member

Ren *et al.*, (2017), carried out an experimental investigation on the structural behavior of concrete-encased concrete-filled steel tube columns under combined compression and torsion. It was revealed that the existence of inner CFST and outer reinforced concrete was a significant effect on the value of the rigidity index, which showed that the rigidity contribution from both the outer reinforced concrete and inner CFST component was comparable. The presence of the outer reinforced concrete or internal CFST part affects the strength index. Result showed that both the outer RC and inner CFST component contribute to the torsional obstruction of the composite members. However, the contribution from the outer RC component is less critical contrasted with that of the internal CFST component. The torsional strength of the concrete-encased CFST column marginally higher than the amount of the torsional strength of confined external RC and inner CFST components. In this manner, the superposition technique was informed for forecasting the torsional strength of the concrete-encased CFST column because of the safe side.

The torsional behavior of concrete encased CFST column was analytically investigated whilst the behavior under combined compression and torsion was studied Li, Han and Hou, (2018).The study indicated that torsional strength of concrete encased CFST was about 2.2-2.8 times of the corresponding RC column. Since the steel tube enhance the torsional capacity. The torsion to rotation angle curve of the inner CFST part was practically equivalent to the relating individual CFST prior to reaching the ultimate strength. Afterward, the sectional twist moment of the inner CFST part was bigger than that of the individual CFST because of the twofold confinement provided by the steel tube and the outer RC component to the core concrete. The material strength in various regions of concrete-encased CFST may influence its performance under combined compression and torsion.

Han *et al*,(2016), was studied the behavior of concrete-encased CFST member under axial tension. It was found that failure mode of the concrete-encased CFST specimen is somewhat similar to that of the RC specimen, but the maximum width of cracks is reduced significantly as a result of the presence of inner CFST. The value of maximum strain for most concrete-encased CFST specimen were smaller than those of the CFST or RC component. It indicates that the deformation ability of concrete-encased CFST specimen was somewhat affected by the premature weld fracture caused by the increased construction complexity.

Huang et al. (2013) was the first to experimentally investigate the pure torsional behavior of HC-SCS columns. The investigation of HC-SCS columns has shown significant strength, ductility, and energy absorption. The investigation revealed the presence of concrete shell enhanced 20% of the column’s torsion capacity. The researchers reported that the concrete shell cracks at 45 º to the axis and maintained its shape. The concrete shell was well bonded with the outer steel tube as no sliding was observed. They reported that the outer steel tube’s strength and thickness were important parameters affecting the torsion behavior.

An, Han and Zhao, (2013) Studied Finite element analysis on the behavior of concrete-encased CFST stub column under axial compression. The load verses axial strain curve of the concrete-encased CFST column can be divided generally in to five stages. When the whole composite column reaches its ultimate strength, the outer reinforced concrete components had reached the ultimate strength. However, the strength of CFST component does not decrease in the whole loading procedure, it approaches to ultimate strength at the peak load of the composite column.

Which mean that the outer RC components sustain most of the applied axial load before ultimate load, while after the inner CFST components sustain most of the applied load.

2.3 Pushout Test

The bond strength is measured by means of pushout test on CFST, CECFST and steel reinforced concrete structures. The steel tube was cut and machined to required length, ensuring that the end of steel tube was normal and regular surface. The outside of steel tube scrubbed to remove rust. The steel tube was larger than the outer reinforced concrete by 50mm at the top and 10mm at the bottom, the steel tube was filled by concrete, the top part of steel tube pushed down in order to investigate the bond stress to slip and load transfer mechanism (Han, Ma and Zhou, 2018).

2.4 Researches Related to Steel-Concrete Interface on Concrete Filled Steel Tube

K.S. Virdi and P.J. Dowling, (1980) were the pioneer to investigate the bond strength of concrete filled steel tube. They carried out push out tests on 76 circular CFST columns. The test parameter was concrete age (7-47 days), concrete compressive strength(24N/mm^2-41N/mm^2), concrete steel interface length (149mm-445mm), tube size or diameter to thickness ratio (17.7-34), concrete compaction (lightly or well compacted), and steel tube interior surface conditions (smooth finish, lubricated and as-received). The test result showed that the bond strength decreased as concrete age increased, surface condition of the steel tube significantly influenced the bond strength, but not obviously influenced by the concrete compressive strength, concrete steel interface length and steel tube interior surface conditions.

Aly *et al.*, (2010) experimentally investigated on 14 circular concrete filled steel tube column specimens had been conducted to study the bond strength behavior of composite column subjected to static loading (on 7 specimens) and variable repeated loading (on 7 specimens). The parameter variables were concrete compressive strength (C40, C60 & C80), age of concrete (28-98days) and the loading protocol (SL & VRL). The result showed that under static pushout loading conditions, the interface bond strength in CFT circular sections with normal strength concrete was discovered to be higher than that with high strength concrete. The age of normal strength concrete was found to initiate a little and moderate decrease in the static and cyclic pushout resistance. The incremental collapse low bound load limit was discovered to be 70% of the static collapse pushout load.

22 pushout tests were carried out to evaluate the concrete steel bond carrying capacity of CFST. The test parameter were concrete strength and diameter of the steel tube. The study showed that the bond strength increased with reduction of the w/c ratio of concrete mixes, resulting in higher bond strength in the case of high strength concrete. The excessive water for high strength concrete was lower than normal concrete; therefore, the effect of shrinkage was less for high strength concrete. For all specimens and concrete mixes, bond strength decreases with increasing of the diameter of the steel tubes. The bond stress-slip curves for the specimens with the same dimensions were similar (Khodaie., 2013).

Qu *et al.*, (2015) Conducted pushout tests on 18 rectangular CFST columns with the point of considering the bond conduct between the steel tube and the concrete infill and the dispersion of the interface bond stress along the part length. The test parameters were concrete compressive strength (C30, C40 and C50), interface length (600,700,800 and 900mm), cross sectional dimension (200*100, 150*100, and 300*200) and interface condition (lubrication and no lubrication). They concluded that the bond strength increases with increasing of concrete compressive strength and decreasing of dimension of steel tube. The lubrication of the steel-concrete interface was shown to induce a significant reduction in bond strength than specimens with no lubrication.

2.5 Researches Related to Steel-Concrete Interface on steel reinforced concrete

Jan A. Wium and Jean-Paul Lebet, (1994) Conducted a pushout test and studied the force transfer from steel to concrete was investigated in composite columns at points of load introduction, considering the influence of concrete cover of the flange, the spacing of horizontal hoop reinforcement, the size of steel section and the shrinkage. The test result showed that an increase in force transfer of 20% was observed after chemical debonding for an increase of concrete cover from 50 mm to 75 mm for an HEB 200 section, an increase in concrete cover from 75mm to 100 mm resulted in an increase of force transfer of 90%. Almost no increase in force transfer due to a thicker concrete cover was observed for HEB 400 sections subjected to high loads. Hoop reinforcement only influences the force transfer after chemical debonding. More concrete cracking occurred for large steel sections, thereby reducing the magnitude of force transferred. Concrete shrinkage reduced the force transfer in the region between the flanges by 10% over a period of six months.

Tao and Yu, (2012) Carried out pushout test on 11 steel reinforced concrete with the aim of investigating the post fire bond between I section steel and concrete. The parameter examined were fire exposure time (0, 90min, 180min), thickness of concrete cover of the flange (60mm, 80mm), concrete compressive strength (25.3MPa, 50.4MPa) and spacing of transverse reinforcement. The test result showed that Significant bond strength decay was seen in SRC columns after fire exposure. Bond strength increments with expanding the thickness of concrete cover for unheated specimens. Nonetheless, for fire-damaged specimens, the impact of the thickness of concrete cover on bond strength was not critical. Bond strength increment with expanding of concrete strength however no undeniable effect on the post-fire bond behavior. Lateral confinement was only effective provided that significant residual expansion occurs for concrete experienced long fire exposure.

2.6 Researches Related to Steel-Concrete Interface on CE-CFST

Han *et al.*, (2016) was conducted total of 3 push-out tests and investigated interface interaction between steel tube and outer concrete of concrete encased CFST column. The variables studied were Strength of the outer concrete (61.5 and 72 N/mm^2) and Diameter of the steel tube (121 and 159 mm). the study verified that the bond strength between the steel tube and outer concrete ranged from 2.96 to 4.44 N/mm^2 and was generally larger than that between the steel tube and core concrete in a CFST column. The bond strength increased with increasing outer concrete strength or decreasing diameter of the steel tube. Average bond strength (3.63 MPa) between the steel tube and outer concrete was used in the finite element method based on the test results.

2.7 Bond Strength

Pushout tests were usually adapted to predict the interaction between steel-concrete in CE-CFST specimens. Average bond stress was used to evaluate the bond behavior between a steel tube and its concrete, which is the push load divided by the area of the interface. Although the distribution of local bond stress along a tube and across its perimeter may not be uniform, the concept of average bond stress is simple to obtain bond strength.

Roeder *et al.*, (1999) investigated the bond between the circular steel tube and concrete, where bond stress capacity was defined as the average interface stress associated with the initial rigid body slip of the concrete core relative to the steel tube. According to Roeder et al. (1999), The behavior of concrete was of rigid body movement between the core concrete and the steel tube with decreasing mechanical resistances from interface shear after the slip was more prominent than that at the ultimate load. Therefore, maximum average bond stress was utilized by many researchers. To further, the axial load gradients are related by statics to the interface bond stress distribution. Thus, if Ps is the axial load in the steel tube at location x, D diameter of steel tube, t thickness of steel tube, then the bond stress, fs(x), is given by

$$f_s(x) = \frac{dP_S}{\pi(D-2t).d_x} \tag{2. 1}$$

Tao *et al.*, (2011) obtained 3 types of average bond stress versus loaded-end slip curves shown in Fig 2.1. The first type of curve is the type A curve, which shows the linear elastic response from 0 to A, the bond stress to slip curve at point A is 50% to 80% of peak bond strength. Then the curve tends to slightly decrease from point A to B (peak bond strength). After reaching the peak bond strength, the curve rapidly declines from point B to C. Then the curve tends to be relatively stable residual bond strength. From point C to D, the bond strength slightly increases. The second type of curve is the type B curve, which shows the linear elastic response from 0 to A, the bond stress to slip curve at point A is 40% to 80% of peak bond strength. After that, the curve tends slightly decrease from point A to B (peak bond strength). After reaching the peak bond strength, the curve rapidly declines from point B to C. Then the curve tends to be relatively stable residual bond strength. The bond strength flattens approach from point C to D. The third type of curve is the type C curve. The bond stress to slip curve is characterized by the lacking of any falling branch. Type C curve shows linear elastic up to point A, 60% to 80% of peak bond stress. Then there will be decreasing in stiffness up to point B (ultimate bond strength). After reaching pt B, the curve continues increasing with an inelastic response up to point C.

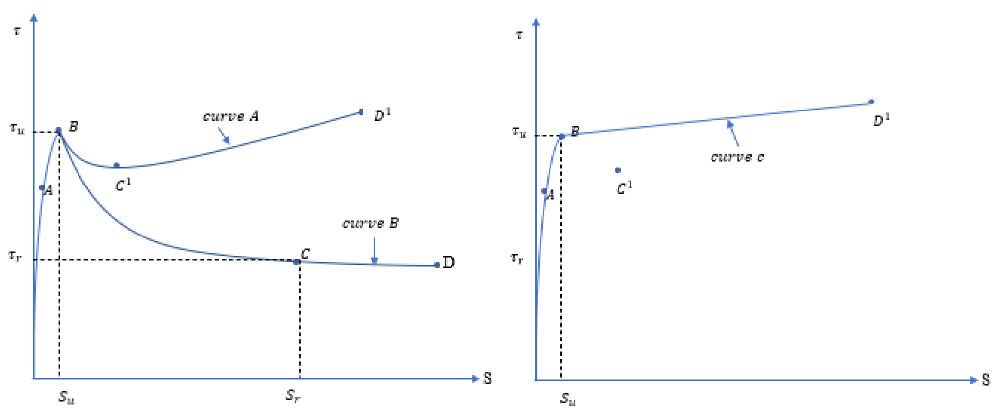

Fig 2. 1 Idealized model of average bond stress versus slip curves

2.8 Bond mechanism

K.S. Virdi and P.J. Dowling, (1980) identified that the resistance to push out loads in filled tubes derived primarily from the interlocking of concrete in two types of imperfections in steel. The first related to the surface roughness of steel and the second to variation in the shape of the cross section, away from the ideal cylindrical surface. The interlocking of concrete in the surface roughness of steel, that is micro-locking, contributes to the useful component of the ultimate bond strength related to the initially stiff region of the load deflection characteristics obtained from the tests. This bond was broken when the concrete interfaces attain a local strain of 0.0035 associated with the compressive crushing of concrete. This component of bond resistance was distinguished from the resistance obtained due to the interlocking of the concrete in the undulating surface of steel due to manufacturing tolerances. This latter type of interlocking, termed macro-locking, was related to the later stages of the load deflection characteristics associated with the primarily frictional movement. The remarkably parallel nature of the characteristics in this region tends to confirm this relationship. This was further supported by tests on smooth and cylindrical inner surface and showed a total absence of macro-locking. It was found that by better compaction both micro locking and macro locking could be enhanced resulting in higher values of ultimate bond strength.

Tao *et al.*, (2011) strengthen the bond mechanism identified by (K.S. Virdi and P.J. Dowling, 1980) that in the elastic stage, the bond resistance was contributed mainly by chemical adhesion and friction. The chemical adhesion was only active in the initial loading stage since the average loaded end slip at the end of elastic stage. Although the microinterlocking mechanism also starts to work in this stage after the slip initiates at the top. After the eminent slippage happened at the free end, the second stage of behavior develops characterized by a gradual reduction of the stiffness of bond stress to the slip curve. The explanation was that the adhesion was presently negligible, and the bond capacity coming from the friction starts to lessen too. The friction reduction could be ascribed to the shearing off mortar which extends into small pits in the steel tube. Then, the macro-interlocking starts to play an important role in this stage After the ultimate bond strength had been accomplished, the third phase of behavior develops, during which the contact was reducing quickly by and large while the bond resistance from macro-interlocking continues to increment.

Qu *et al.*, (2013) conducted load-reversed push-out tests on 6 rectangular CFST columns with the aim of investigating the nature of the bond between the concrete infill and the steel tube. The research revealed that Macro-locking was found to be the dominant mechanism contributing to bond strength, followed by micro-locking, whereas the effect of chemical adhesion appeared to be limited as shown in Fig 2.2.

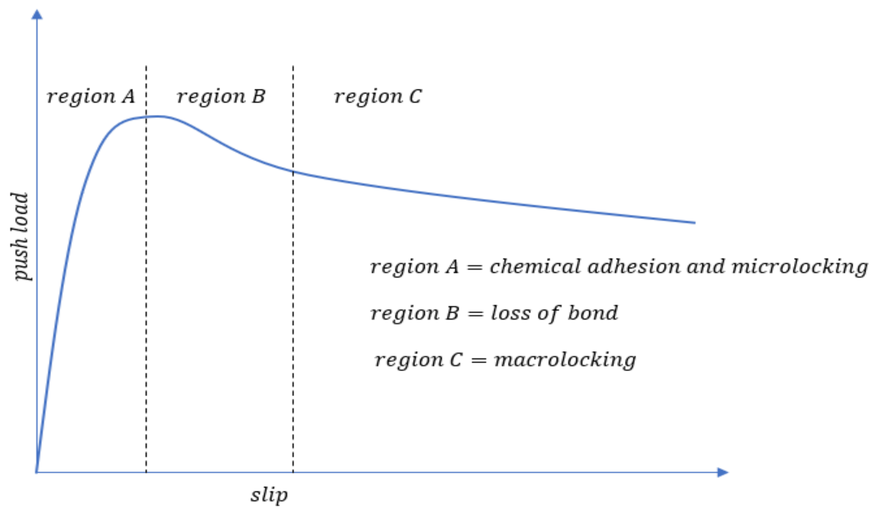

Fig 2. 2 Idealized response of push-out specimens

Feng *et al.*, (2018) investigated bond strength of concrete-filled stainless steel SHS tubes by conducting pushout test. The author found that shear failure loads of bonding slip diminished with additional loading cycles of the repeated push-out test utilized in the same way, which demonstrated that the mechanical interlock load was continuously weakened. likewise, 70% of the bonding strength at the interface was taken by the friction force of the interface components, while the remaining 30% of the bonding strength at the interface was sustained by the chemical adhesive force and the mechanical interlock force.

2.9 Design Codes

Eurocode 4, (2004), ES-EN1994,(2015), For axially loaded columns and compression members, longitudinal shear outside the areas of load introduction need not be considered. Outside the area of load introduction, longitudinal shear at the interface between concrete and steel should be verified where it is caused by transverse loads and /or end moments. Shear connectors should be provided, based on the distribution of the design value of longitudinal shear, where this exceeds the design shear strength for Concrete filled circular hollow sections is 0.55 N/mm^2 and completely concrete encased steel sections is 0.30 N/mm^2.

CHAPTER 3 EXPERIMENTAL PROGRAM

3.1 General

A total of nine push out test was conducted on circular CE-CFST columns specimens of 460mm height with approximately 400mm steel-concrete interfaces length to investigate the bond performance of steel-concrete interfaces between the circular steel tube and outer concrete of CE-CFST. The Experimental investigation was carried out on nine specimens from nine different mixes of 25MPa, 35MPa, and 45MPa compressive strength of concrete. The parameter variables were concrete compressive strength (25MPa, 35MPa, and 45MPa), concrete cover (60mm and 80mm), and spacing of transverse reinforcement (Ǿ8 c/c 70mm and Ǿ8 c/c 125mm).

Table 3.1 provides the information on test specimens, where D is the diameter of steel tubes, t is the thickness of steel tubes, H and B are the overall cross-sectional size of CE-CFST. The steel tubes used were the same for all specimens, which were cut from a 6-meter length of steel tubes.

Table 3. 1 summery of test specimens

<table>
<tr><th>Specimen Label</th><th>Steel cross section (D*t) (mm)</th><th>Compressive strength (MPa)</th><th>Concrete cover (mm)</th><th>Cross section size (B*H) (mm*mm)</th><th>Spacing of Transverse reinforcement (mm)</th><th>Longtidunal bars (mm)</th></tr>
<tr><td>CECFST 31</td><td>102*3</td><td>25</td><td>80</td><td>220*220</td><td>Ǿ8 c/c 70 mm</td><td>8 Ǿ14mm</td></tr>
<tr><td>CECFST 11</td><td rowspan="4">102*3</td><td rowspan="4">45</td><td rowspan="2">60</td><td>220*220</td><td>Ǿ8 c/c 70 mm</td><td>8 Ǿ14mm</td></tr>
<tr><td>CECFST 12</td><td>220*220</td><td>Ǿ8 c/c 125 mm</td><td>8 Ǿ14mm</td></tr>
<tr><td>CECFST 13</td><td rowspan="2">80</td><td>260*260</td><td>Ǿ8 c/c 70 mm</td><td>8 Ǿ14mm</td></tr>
<tr><td>CECFST 14</td><td>260*260</td><td>Ǿ8 c/c 125 mm</td><td>8 Ǿ14mm</td></tr>
<tr><td>CECFST 21</td><td rowspan="4">102*3</td><td rowspan="4">35</td><td rowspan="2">60</td><td>220*220</td><td>Ǿ8 c/c 70 mm</td><td>8 Ǿ14mm</td></tr>
<tr><td>CECFST 22</td><td>220*220</td><td>Ǿ8 c/c 125 mm</td><td>8 Ǿ14mm</td></tr>
<tr><td>CECFST 23</td><td rowspan="2">80</td><td>260*260</td><td>Ǿ8 c/c 70 mm</td><td>8 Ǿ14mm</td></tr>
<tr><td>CECFST 24</td><td>260*260</td><td>Ǿ8 c/c 125 mm</td><td>8 Ǿ14mm</td></tr>
</table>

3.2 Materials

Concrete-encased CFST column specimens are a composite material made up of concrete and steel materials. The mechanical properties of each material are discussed in the below subtopics.

3.2.1 Concrete

Concrete is a mixture of cement, coarse aggregate, fine aggregate, and water, which harden with time. ACI mix design was conducted to get the needed target cylindrical compressive strength of concrete (25MPa,35MPa and 45MPa). Abebe Dinku (2002) construction laboratory manual was used to investigate material properties of concrete ingredients of cement, coarse aggregate, and fine aggregate.

Fine aggregate

Fine aggregate is the particles that pass through a 4.75mm sieve and retain on 0.075mm sieve and function in concrete to fill the voids between the coarse aggregate. The source of fine aggregate for this research is river sand. It was tested and found to have a specific gravity of 2.31, free surface moisture of 5.29%, fineness modules of 2.61, and water absorption of 4.32%. The silt content of the sand was 3.8% which is below the permissible limit of 6%.

Coarse aggregate

Coarse aggregates are the particle that retains on a 4.75mm sieve and acts as inert filler material for concrete. The source of coarse aggregate for this research is crushed stone. The coarse aggregate was tested and found to have a specific gravity of 2.85, free surface moisture of 1.4%, and water absorption of 0.92%.

Cement

Ordinary Portland cement with 42.5 R strength class was used for the mix of the current research. The specific gravity of OPC is 3.15.

The concrete mix formulated from two main batches of eight mix with a different water-cement ratio as shown in table 3.2. Concrete strength of 25MPa, 35MPa, and 45MPa was used to investigate the effect of concrete strength on the bond performance of concrete-encased CFST column.

Table 3. 2 Mix proportion of concrete ingredients

Concrete strength (MPa)	Nominal aggregate Size (mm)	Cement content (kg/m^3)	Coarse aggregate (kg/m^3)	Fine aggregate (kg/m^3)	Water (kg/m^3)	Water cement ratio
25	19	410.0	1022.67	751.46	193.09	0.54
35	19	436.17	1022.67	731.25	193.42	0.47
45	19	569.44	1022.67	628.35	194.37	0.37

Three 150*150*150 mm cubes were prepared for every nine mixes. As shown in the Fig 3.1, a Slump was taken for each mix to preserve the consistency of concrete work. The specimen mold was filled in three layers and compacted using a vibrating table. The concrete-encased CFST specimens were demolded after one day/ 24 hours then placed in a water tank vertically. Before testing, the specimens were removed from the water tank and tested the compressive strength and result presented in Table 3.3.

Fig 3. 1 Concrete slump test

Table 3. 3 cube compressive strength

Specimens	Testing day	Weight (gm)	Compressive Strength (MPa)	Average compressive strength (MPa)
CE-CFST 31	52	7612	27.25	25.97
		7732	23.99	
		7653	26.68	
CE-CFST 11	38	7853	47.74	46.96
		7870	46.93	
		7908	46.23	
CE-CFST 12	38	8085	42.85	45.97
		7963	45.66	
		7999	49.39	
CE-CFST 13	38	7938	46.5	48.13
		8024	49.63	
		8021	48.26	
CE-CFST 14	38	7893	44.92	46.04
		7873	40.45	
		7924	52.74	
CE-CFST 21	38	7857	36.15	34.57
		7807	34.2	
		7828	33.35	
CE-CFST 22	38	7832	37.08	37.116
		7894	37.39	
		7865	36.88	
CE-CFST 23	38	7855	34.24	36.08
		7915	38.09	
		7866	35.92	
CE-CFST 24	38	8011	32.29	34.30
		7841	35.88	
		7970	34.73	

3.2.2 Reinforcement

The diameter of 8mm and 14mm deformed reinforcement was used for longitudinal and transverse rebars, respectively. The nominal yield strength for longitudinal reinforcement was 529.59MPa, whereas for the transverse rebars was 447.56MPa.

A universal testing machine with a tensile capacity of 1000kN was used to measure the mechanical properties of reinforcement. Three samples of the bar were taken for the uniaxial tensile test. Mechanical properties of reinforcement were present in Table 3.4.

Table 3. 4 Mechanical properties of Reinforcement

$Diameter$ (mm)	$Yield$ $load$ (kN)	$Failure$ $load$ (kN)	$Elongation$ (%)	$Yield$ $stress$ (MPa)	$Failure$ $stress$ (MPa)	$Average$ yield stress (MPa)	$Average$ $failure$ stress (MPa)
8	25.8	33.2	23.5	442.32	569.19	447.56	562.75
	26.4	32.8	23.6	450.51	559.73		
	26.3	32.7	23.6	449.85	559.32		
14	90.2	106.5	22.5	533.19	629.55	529.59	635.49
	89.7	108.2	22.7	528.80	637.86		
	89.6	108.7	22.5	526.77	639.06		

3.2.3 Steel tube

The steel tube used for the experiment was a circular hollow carbon steel section with an outer diameter of 102mm and 3mm wall thickness adopted for all concrete-encased CFST column specimens. Three steel samples were taken from the steel tube and tested. The standard tensile test was conducted to measure the material properties of the steel tube shown in Fig 3.2. The yield strength of the steel tube was 309.2MPa with a mean value and standard deviation of 38.53%, which is greater than the coefficient of variation (15%). So, one sample result scattered from the mean value will be ignored. The yield stress will be taken as 282.05MPa with a 3.23% standard deviation. The mechanical properties of the steel tube are discussed in Table 3.5.

Table 3. 5 Mechanical properties of steel tube

$Diameter$ (mm)	Thickness (mm)	$Yield$ $load$ (kN)	$ultimate$ $load$ (kN)	$Elongation$ (%)	$Yield$ $stress$ (MPa)	$Failure$ stress (MPa)	$Average$ yield stress (MPa)	$Average$ failure stress (MPa)
102	3	12.2	13.6	27	363.5	405.2	282.05	491.60
	3	9.6	16.4	24	286	488.6		
	3	9.3	16.6	28	278.1	494.6		

Fig 3. 2 Tensile test on steel tubes

3.3 Specimen's Fabrication

3.3.1 Formwork

Plywood was used for the fabrication of formwork. To prevent the bursting of formwork during vibration, the side of the formwork was confined by zigba, and during casting additional confinement was provided by C-clamp. The bottom plywood was cut circularly at the center as shown in Fig 3.3. The inner surface of the formwork was sprayed with oil to remove the formwork easily after the concrete harden.

Fig 3. 3 formwork

3.3.2 Reinforcement

All column specimens were longitudinally reinforced with an eight 14mm diameter bar shown in Fig 3.4. However, two types of stirrups arrangement used for transverse reinforcement, while 8mm diameter stirrups with 70mm and 125mm spacing, were used to investigate the effect of lateral confinement of concrete on bond strength.


Fig 3. 4 reinforcement preparation

3.3.3 Steel Tube

Six-meter length of steel tube was cut and machined to 460mm length shown in Fig 3.5. The inside and outside surfaces of the steel tube were wire scrubbed to remove any corrosion. Any deposit of grease and oil was cleaned away.

3.3.4 Test Sample Preparation

The steel profiles were as received from the manufacturer, and no specific measures were taken to treat the surfaces. All specimens were cast in the upright position, and plywood molds were used. The cast specimens were then cured in the laboratory. After being cured for about 38 days, Push-out test was conducted. The cross-sectional dimension of specimens was shown in Fig 3.6. Group 1 sample includes four specimens with 45MPa compressive strength and the sectional dimension of 220mm*220mm and 260*260mm. Group 2 sample includes four specimens with 35MPa compressive strength and the sectional dimension of 220mm*220mm and 260*260mm. one sample with the dimension of 260*260mm and 25MPa compressive strength.

Fig 3. 5 Cut and machined steel tube

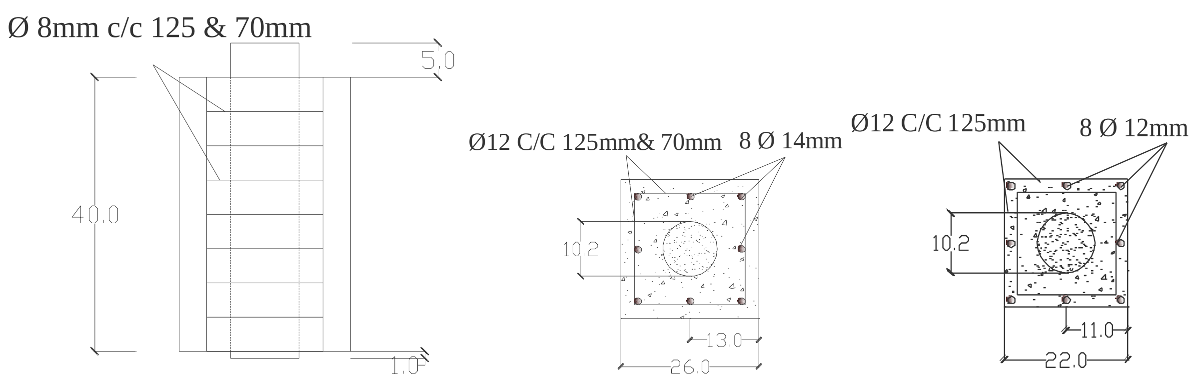

Fig 3. 6 Cross-sectional dimension of specimen

3.4 Test Setup and Instrumentation

The push-out test setup is shown in Fig 3.9 to apply load uniformly to the top surface of CFST, the top surface grounded to provide a level surface. 400kN capacity of the testing machine was used. The CE-CFST specimen were placed vertically on a rigid square plate. The rigid plate was pre-cut on the center to allow downward movement of CFST. Most of the bottom outer RC part was supported by the steel plate shown in Fig 3.7. The CFST was 50mm and 10mm longer than the outer RC on the top and bottom, respectively. The additional 10mm length of CFST at the bottom was provided to place centrally on the rigid base plate. The load cell is placed on the top of CFST to measure the applied load. The specimen was confined by strophiole for stability of the loading system.

Fig 3. 7 Steel plate

For all specimen's force-controlled method was used. The relative slip of CFST to outer RC was measured by the linear variable transducer. Two transducers were used to measure the slip of the specimens on the loading end(top). To measure the load transfer mechanism from the steel tube to the outer RC, strain gauges were installed on the outer surface of the RC. Three strain gauges were installed along the length of RC for all specimen to measure longitudinal strain and three strain gauges were installed horizontally to measure hoop strain on the concrete surface of two specimens shown in Fig 3.8.

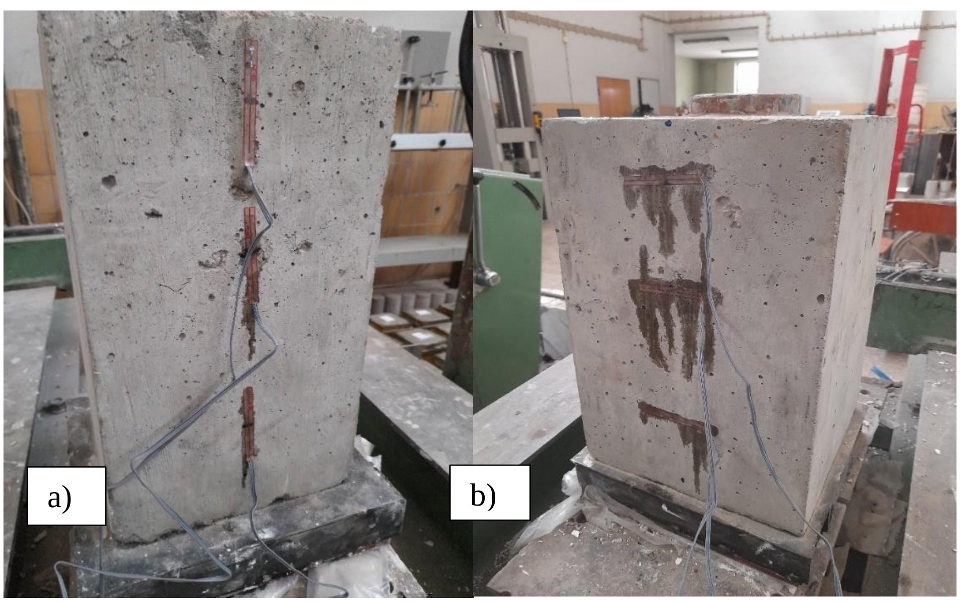

Fig 3. 8 strain gauges arrangment a) Longitudinal strain gauge b) transverse strain gauge

The loading was ended when the slip reaches 45mm. Data come from loading cell (reaction force), linear variable transducer, and strain gauges were recorded and stored by data logger shown in Fig 3.8.

Fig 3. 9 push out setup

CHAPTER 4. FINITE ELEMENT MODELING

4.1 General

The finite element program ABAQUS is conducted to simulate the push-out test of debonding of steel concrete interfaces in concrete-encased concrete-filled steel tube. The finite element model consists of different materials such as; concrete, steel tube, longitudinal reinforcement, lateral reinforcement, rigid plate, and cohesive material property. Due to the different confinement of concrete, the concrete can be zoned into three regions. Those are core concrete confined by steel tube, outer confined concrete confined by lateral reinforcement, and unconfined outer concrete. The interaction between the steel tube and outer concrete was adopted by considering the chemical adhesion, normal contact, and tangential friction.

4.2 Concrete Material Modeling

The finite element model of Concrete in CE-CFST can be classified into three zones based on the confinement of transverse reinforcement and steel tube: those are unconfined outer concrete, confined outer concrete, and core concrete shown in Fig 4.1. Concrete damage plasticity(CDP) was used to define compressive damage and tensile crack of concrete in (Abaqus). Different stress-strain relations are applied depending on zones.

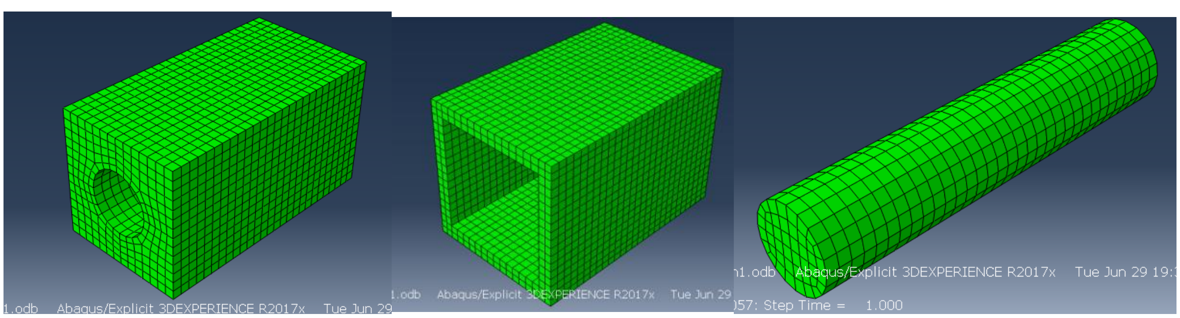

A, Outer confined concrete   B, Outer unconfined concrete C, core concrete

Fig 4. 1 Types of concrete based on the confinement

4.2.1 Outer Unconfined Concrete

The damage plasticity model is used to describe the constitute behavior of concrete provided by Abaqus. A stress-strain model of unconfined concrete proposed by EC2 is used for the uniaxial compressive stress-strain relation of outer unconfined concrete. The compressive stress-strain curve has three parts. In the first part, the stress-strain curve rise elastic linearly up to $0.4fck$, where fck is the compressive cylinder strength of concrete, and strain (ε_{c1}) at $0.4fck$ is 0.00052, given by EC2.

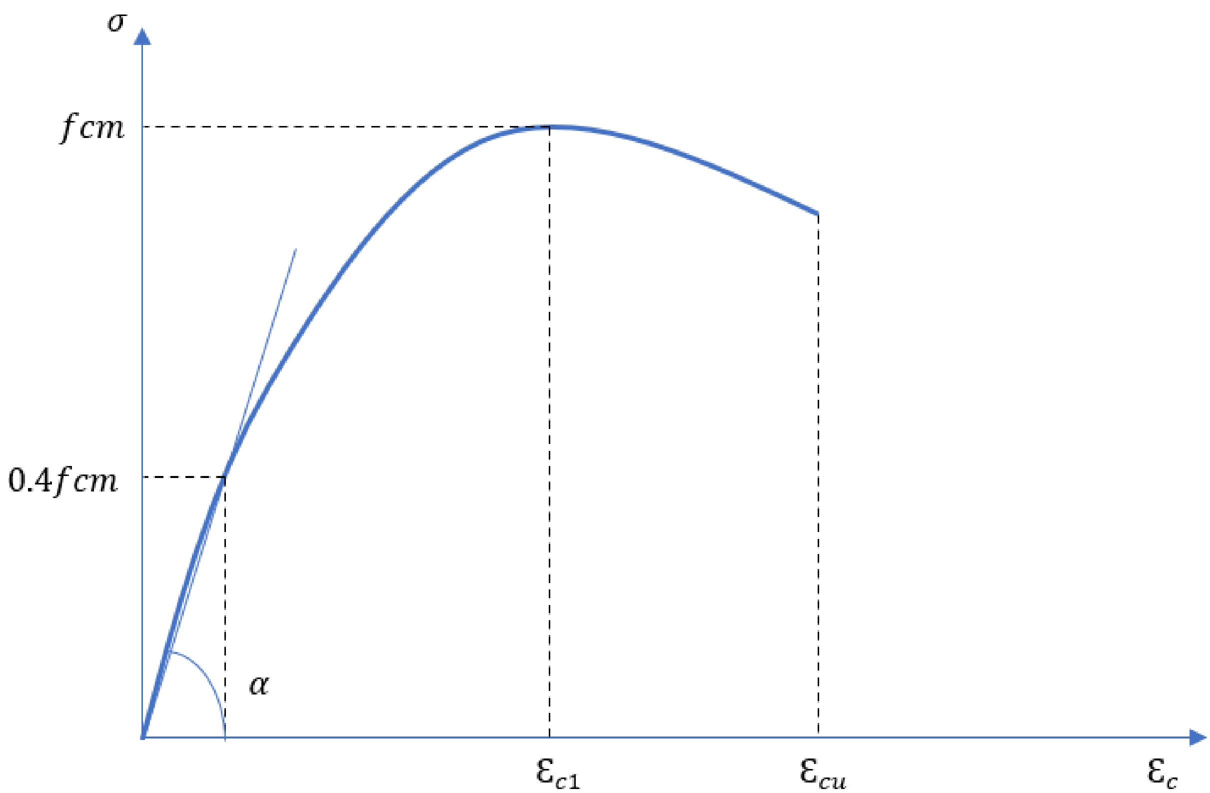

Fig 4. 2 Stress-strain curve of unconfined outer concrete

The second part of the curve starts from $0.4fck$ to the peak point fck with the non-linearly parabolic curve. When the stress reached the peak point, the strain is 0.0023. The equation of the parabolic curve can be calculated by the following equation.

$$\frac{\sigma c}{fcm} = \frac{k\eta - \eta^2}{1+(k-2)\eta} \quad (4.\ 1)$$

Where,

$$\eta = {}^{\varepsilon c}/_{\varepsilon c1} \quad (4.\ 2)$$

$\varepsilon c1 = 0.0023$

$$k = \frac{1.05 * Ecm * |\varepsilon c1|}{fcm} \quad (4.\ 3)$$

In the third part, the stress-strain curve has decreased from the peak point to $0.85fck$. The ultimate strain at the $0.85fck$ is taken as 0.0035. But for this research, different values of ultimate strain were tried and good results were found at the ultimate strain of 0.004. The elastic modulus of concrete is taken as $22 * \left(\frac{fcm}{10}\right)^{0.3}$ according to EC2, where fcm is concrete cylinder compressive strength and Poisson ratio taken as 0.2.

4.2.2 Outer Confined Concrete

Due to the confinement of transverse reinforcement, the concrete under the stirrups zoned to outer confined concrete, as shown in Fig 4.3. The confinement of stirrups increases the plasticity of concrete, which was influenced by the volumetric stirrups ratio, the yield stress of stirrups, and the compressive strength of concrete by Han and An, (2014).

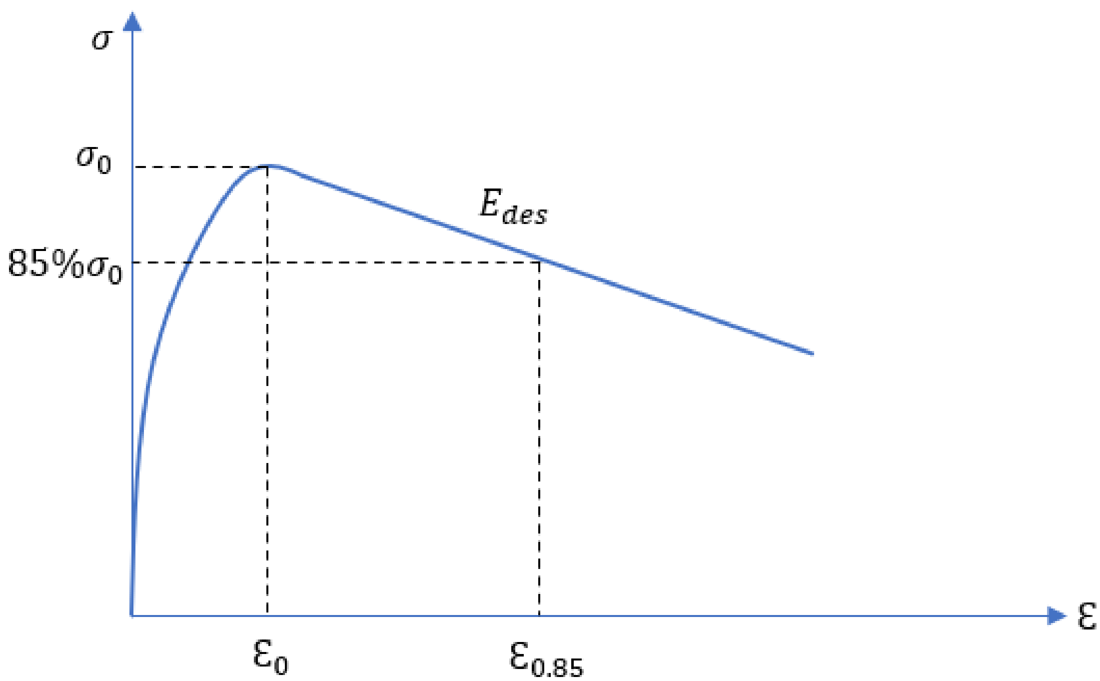

Fig 4. 3 Stress-strain curves of outer unconfined concrete

Uniaxial stress-strain model for outer confined concrete has two regions. In the first region, the stress and strain increase up to the peak point presented by Popovics, (1973). The relation between stress to strain in the first part can be calculated by the following equation.

$$\sigma = \sigma_0 * \frac{k*\left(\frac{\varepsilon}{\varepsilon_0}\right)}{k-1+\left(\frac{\varepsilon}{\varepsilon_0}\right)^k} \qquad \text{for } \varepsilon \leq \varepsilon_0 \qquad (4.\ 4)$$

In the second region, the stress-strain curve linearly decreased from the peak point to the failure point. The falling branch of the curve is idealized by a straight line, characterized by equation. The deterioration rate (E_{des}) is descending slope from maximum stress to 85% of the maximum stress corresponding to strain to account volumetric stirrups ratio, sectional width, and stirrup spacing. Which is developed from regression analysis of test data in the range of ε_0 and ε_{cu} presented by Hoshikuma *et al.*, (1997).

$$\sigma = \sigma_0 - E_{des}(\varepsilon - \varepsilon_0) \qquad \text{for } \varepsilon > \varepsilon_0 \tag{4. 5}$$

In which, $\sigma_0 = f_c$

$$k = \frac{E_c}{E_c - {\sigma_0}/{\varepsilon_0}} \tag{4. 6}$$

$$\varepsilon_0 = 0.00245 + 0.0122 * \frac{\rho_v * f_{yh}}{f_c} \tag{4. 7}$$

$$E_{des} = \frac{0.15 * \sigma_0}{\varepsilon_{0.85} - \varepsilon_0} \tag{4. 8}$$

$$\varepsilon_{0.85} = 0.225 * \rho_v * \sqrt{\frac{B_c}{S}} + \varepsilon_0 \tag{4. 9}$$

$$\rho_v = \frac{A_h l_h}{A_0 * S} \tag{4. 10}$$

ρ_v is stirrups ratio, $A_h$is cross-sectional area of stirrups, l_h is total length of stirrups, A_0 is area of confined concrete, f_{yh} is yield stress of stirrups, S is the stirrups spacing and B_c is the sectional width of confined concrete.

4.2.3 Core Concrete

The strength and the plasticity of confined concrete increase contrasted to the unconfined concrete. In the concrete damage plasticity model, the strength improvement at the state of triaxial loading can be accomplished by the definition of the yielding surface and the equivalent uniaxial stress-strain relationship was used to represent the plastic behavior of core concrete. The plasticity of core concrete increase due to the confinement of the steel tube, which influenced by the confinement factor ξ, expressed by Han, Yao and Tao (2007).

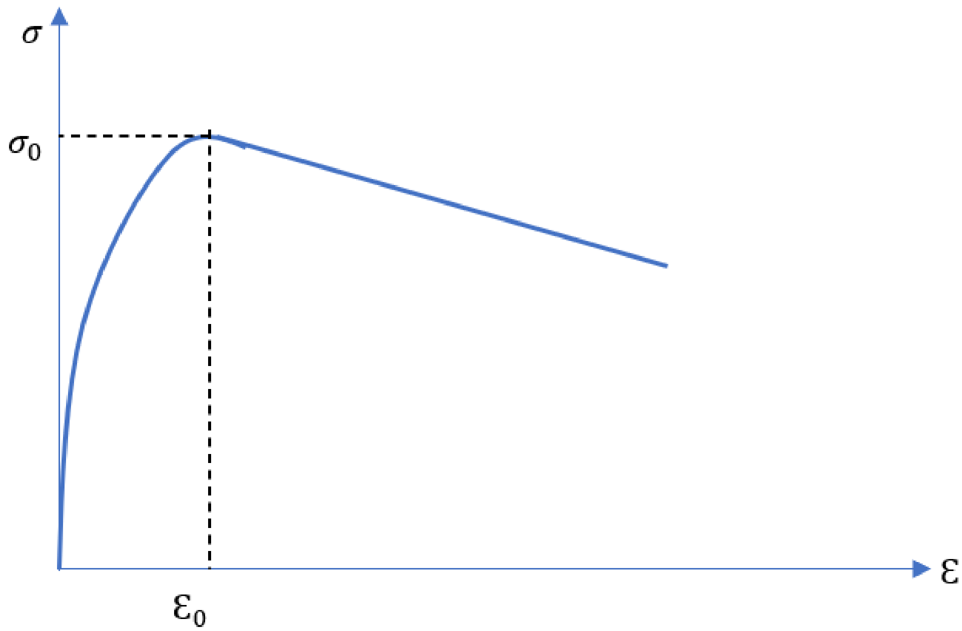

Fig 4. 4 Stress-strain curve of core concrete

$\xi = \frac{A_s f_y}{A_{core} f_{ck,core}}$, where A_s is the cross-sectional area of steel tube, A_{core} is the cross-sectional area of core concrete, f_y is yield stress of steel tube, and is the characteristic strength of concrete. The uniaxial stress-strain curve has two principal locales: the first region, the strain relating to the maximum stress will increases. On the subsequent region, the descending part of stress-strain curves tends to even. The equivalent stress strain can be expressed by Han, Yao and Tao, (2007).

$$\frac{\sigma}{\sigma_0} = \begin{cases} \frac{2\varepsilon}{\varepsilon_0} - \left(\frac{\varepsilon}{\varepsilon_0}\right)^2 & for\ \varepsilon \le \varepsilon_0 \\ \frac{\varepsilon/\varepsilon_0}{\beta_0\left(\varepsilon/\varepsilon_0 - 1\right)^{\eta} + \varepsilon/\varepsilon_0} & for\ \varepsilon > \varepsilon_0 \end{cases} \tag{4. 11}$$

$$\sigma_0 = f_c \tag{4. 12}$$

$$\varepsilon_0 = \varepsilon_c + 800\xi^{0.2} * 10^{-6} \tag{4. 13}$$

$$\varepsilon_c = (1300 + 12.5 f_c) * 10^{-6} \tag{4. 14}$$

$$\eta = 2\ for\ CFST\ with\ circular\ section$$

$$\beta_0 = (2.36 * 10^{-5})^{(0.25+(\xi-0.5)^7)} * (f_c)^{0.5} * 0.5 \ge 0.12\ for\ CFST\ with\ circular\ section$$

f_c is cylindrical strength of concrete.

Failure of concrete both in tensile cracking and compression damage is modeled by concrete damage plasticity. CDP is based on a plastic-based continuous damage model. The uniaxial compressive damage coefficient d_c is used to define concrete stiffness degradation by the following equation. Where, ${\varepsilon_c}^{pl}$is plastic strain, which increases proportionally with inelastic strain (${\varepsilon_c}^{in}$), b_c is the ratio of plastic strain to inelastic strain ($b_c = 0.7$). The evolution of the compressive damage component d_c is linked to the corresponding plastic strain ${\varepsilon_c}^{pl}$ which is determined proportional to the inelastic strain ${\varepsilon_c}^{in}= \varepsilon_c - \sigma c/Ec$ using a constant factor b_c by Birtel, Mark and Bochum, (2006).

$$d_c = 1 - \frac{\sigma_c}{E_c {\varepsilon_c}^{pl}\left(1/_{b_c} - 1\right) + \sigma_c} \qquad (4.\ 15)$$

The tensile stress increases elastically without cracking up to the critical tensile stress. After reaching peak stress, a crack will develop on the concrete surface. The tensile behavior of concrete given by;

$$\sigma_t = E_c \varepsilon_t \ \text{ if } \varepsilon_t \leq \varepsilon_{cr} \qquad (4.\ 16)$$

$$\sigma_t = f_{ctm}\left(\frac{\varepsilon_{cr}}{\varepsilon_t}\right)^{0.4} \text{ if } \varepsilon_t > \varepsilon_{cr}, \quad f_{ctm} = 0.3 * {f_{ck}}^{2/3} \qquad (4.\ 17)$$

Tensile stiffness degradation can be calculated by:

$$d_t = 1 - \frac{\sigma_t}{E_c {\varepsilon_c}^{pl}\left(1/_{b_t} - 1\right) + \sigma_t}, \ b_t = 0.1 \qquad (4.\ 18)$$

The yield surface of concrete after the elastic limit defined by the Drucker-Prager yield criterion model. Drucker-Prager yield criterion model is a pressure-dependent model for determining whether a material has failed or undergone plastic yielding. In Abaqus the parameter required to define the yield surface consists of five constitute behavior based on the sensitive analysis of concrete. The Poisson’s ratio controls the volume change of concrete for stress below the critical value which is the onset of inelastic behavior. Once the critical stress values reached concrete exhibits an increase in plastic volume under pressure. This behavior is considered by defining parameter. The first parameter is dilation angle(ψ) and it defines the angle of internal friction of the material, which measured in the p-q plane at high confine pressure as shown in fig 4.5. The value dilation angle(ψ) is 30^0 (Abaqus user manual) and its shows the direction of the plastic strain increment vector. The second parameter is eccentricity(e) and it defines the rate at which the hyperbolic flow potential approaches its asymptotes, which is equal to 0.1 (default value from Abaqus user manual).

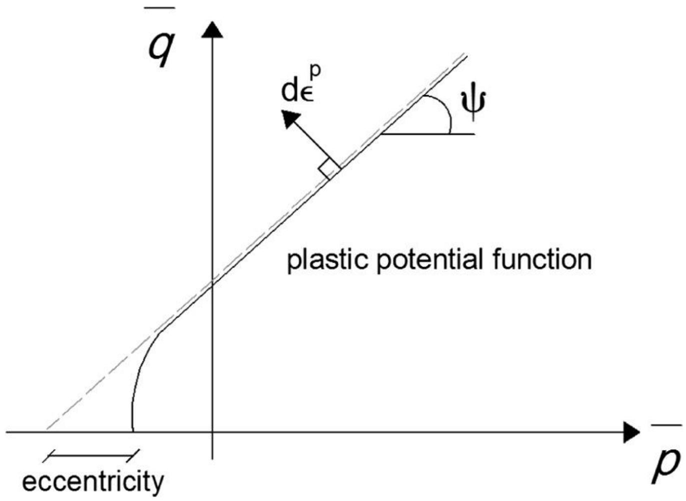

Fig 4. 5 dilation angle and eccentricity in meridian plane

The third parameter is the ratio biaxial to uniaxial compressive strength (σ_{bo}/σ_{co}) is 1.16 (default value from Abaqus user manual). The fourth parameter is the ratio of flow stress in the tensile meridian to the compressive meridian and defines the shape of yield surface in the deviatory plane (Kc) is given by 0.667 (default value from Abaqus user manual) shown in fig 4.6. The fifth parameter is viscosity (μ) and defines the vesco-plastic regularization of the concrete constitutive equation, which is the value of 0 (default value from Abaqus user manual).

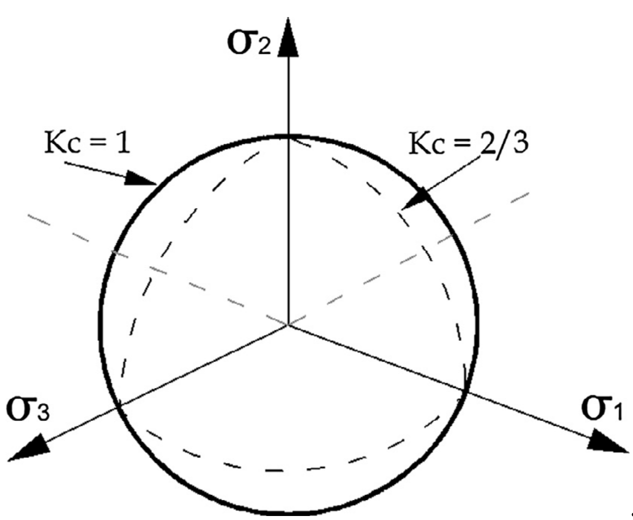

Fig 4. 6 Yield surfaces in the deviatory plane

4.3 Steel Material Modeling

Fig 4.7 shows, the bilinear stress to strain model was utilized to indicate the stress to strain curve for reinforcement bar. The modulus elasticity of reinforcement in linear region taken as Es.

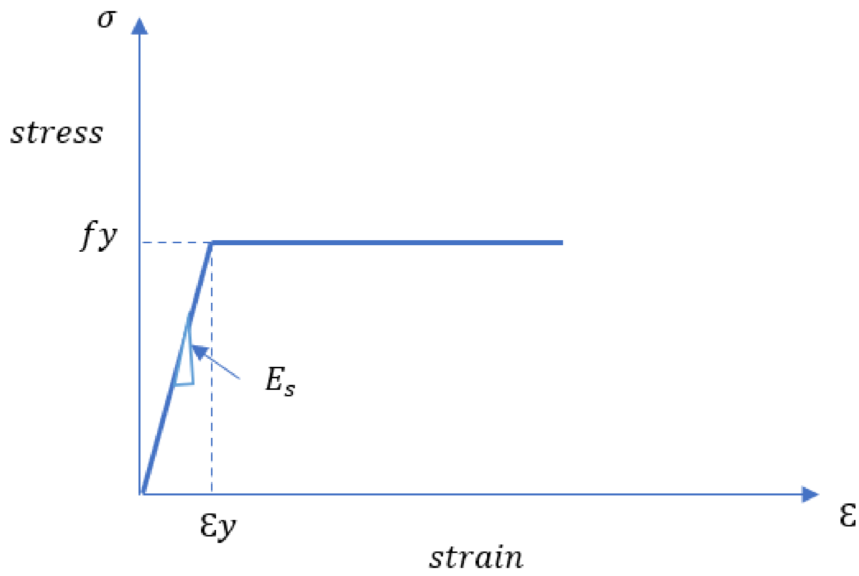

Fig 4. 7 Bilinear stress-strain curve of bars

A trilinear stress-strain relation was adopted to simulate the steel tube as shown in fig 4.8. The yield stress and the ultimate stress are taken from material test as 282.05MPa and 462.8MPa, respectively. The elastic modulus and Poisson ratio were 200GPa & 0.3, respectively.

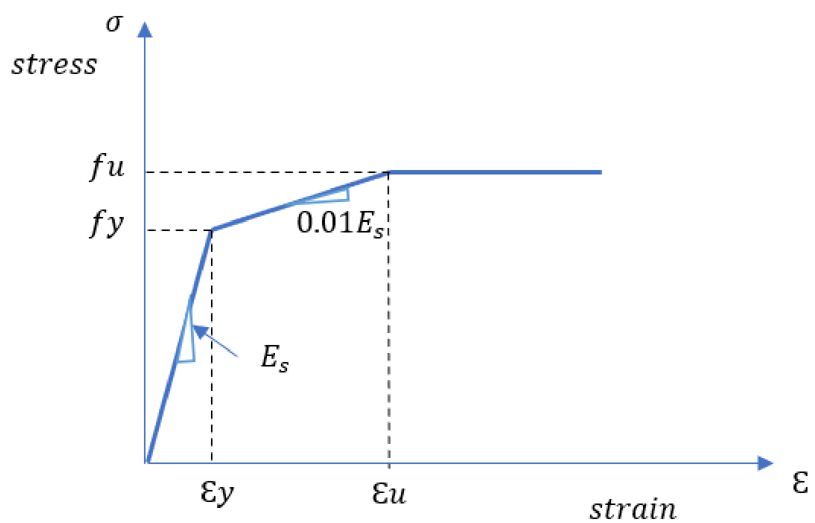

Fig 4. 8 Trilinear stress-strain curve of steel tube

4.4 Cohesive Property Modeling

Cohesive material properties used between the steel surface and concrete surface to model the natural bond strength, in ABAQUS. Bilinear traction separation law used to assume the traction in normal and two tangential directions to the corresponding separation. Fig 4.9 shows Traction to separation law starts with linear elastic behavior up to the initiation of damage. After reaching the initiation damage, there will be the development of separation between interfaces. Then evolution will proceed up to full separation.

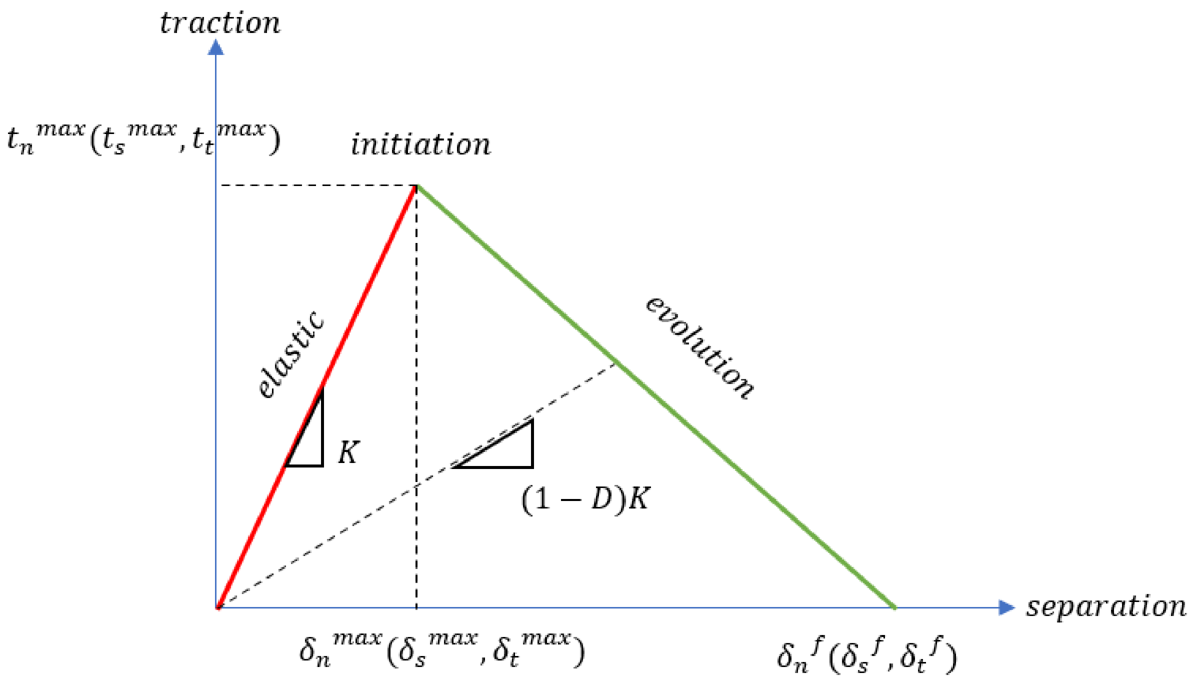

Fig 4. 9 Traction separation curve of cohesive property

Uncoupled traction matrix was used to define the elastic linear region. Where t_n, t_s and t_t are traction stress in the normal, and two tangential directions, K_{nn}, K_{ss} and K_{tt} are stiffness of cohesive layer in the normal, and two tangential directions, δ_n, δ_s and δ_t are separation of cohesive layer in the normal, and two tangential directions. The value of $K_{nn} = 65\text{MPa}/mm$, $K_{ss} = 25\text{MPa}/mm$ and $K_{tt} = 25\text{MPa}/mm$ conducted by Wang *et al.*, (2019).

$$t = \begin{Bmatrix} t_n \\ t_s \\ t_t \end{Bmatrix} = \begin{bmatrix} K_{nn} & 0 & 0 \\ 0 & K_{ss} & 0 \\ 0 & 0 & K_{tt} \end{bmatrix} \begin{Bmatrix} \delta_n \\ \delta_s \\ \delta_t \end{Bmatrix} \tag{4. 19}$$

For damage initiation criterion of traction separation model, the quadratic separation criterion is used to define the peak separation in normal and tangential direction is presented by ${\delta_n}^{max}$, ${\delta_s}^{max}$ and ${\delta_t}^{max}$, which have value of 0.025mm, 0.06mm and 0.06mm, respectively, investigated by Lee *et al.*, (2011), shown in the equation, where < > represent Macaulay bracket, which shows compression do not initiate damage. Whereas, if t_n>0 (tension), <δ_n> = δ_n, and <δ_n>=0 otherwise.

$$\left(\frac{<\delta_n>}{{\delta_n}^{max}}\right)^2 + \left(\frac{\delta_s}{{\delta_s}^{max}}\right)^2 + \left(\frac{\delta_t}{{\delta_t}^{max}}\right)^2 = 1 \tag{4. 20}$$

For surface based cohesive behavior, linear softening law used to define the decrease in cohesive stiffness after the initiation criterion reached. The slope of damage evolution(D) is given by equation.

$$D = \frac{{\delta_m}^f\left({\delta_m}^{max} - {\delta_m}^o\right)}{{\delta_m}^{max}\left({\delta_m}^f - {\delta_m}^o\right)} \tag{4. 21}$$

Where ${\delta_m}^f$ is the maximum separation at which the cohesive layer failed, which is equal to 2.5mm was used for the simulation; ${\delta_m}^{max}$ is the maximum separation reached during the loading process; ${\delta_m}^o$ is the effective separation at the cohesive damage initiation.

4.5 Finite Element Type and Mesh

The finite element model is composed of six materials. Those are outer unconfined concrete, outer confined concrete, core confined concrete, steel tube, reinforcement bar, load plate, and rigid plate. Each element is modeled independently by part. A structured meshing technique was used for the appropriate element shape. Partitioning and local mesh seeds allow to refine the mesh in the area of a stress concentration where greater accuracy is needed, especially if the shape of modelled structures is complex. As illustrated in Fig 4.10, 3-dimensional 8-node reduced integration solid element C3D8R was used to simulate the outer unconfined concrete, outer confined concrete, and core confined concrete section. Outer RC and core concrete were meshed by a controlled global size of 15mm and 14mm, respectively. Truss element T3D2 was used to model the reinforcement bar. The truss element meshed by a controlled global size of 17mm. Four nodes of conventional shell elements S4R were used to model the steel tube. Shell element was meshed by a controlled global size of 14mm. Rigid element R3D4 was used to model the base plate & load plate, meshed by a controlled global size of 15mm. Diverse mesh sizes are attempted to achieve harmony among accuracy and efficiency for modeling. A maximum mesh size of 17mm is used for modeling, and a fine mesh size of 14mm is used.

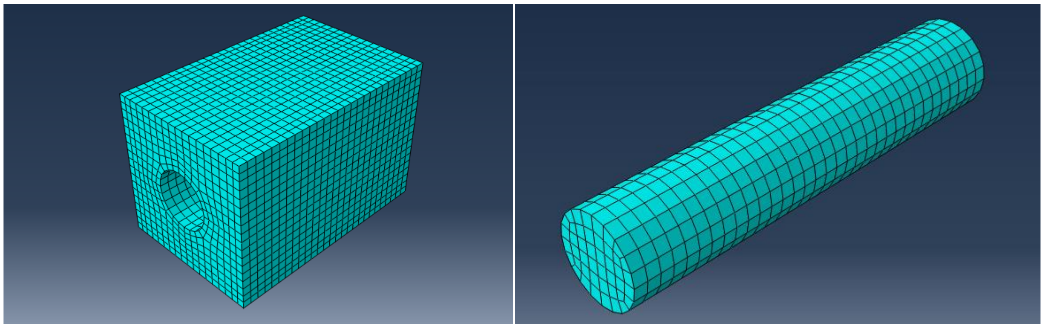

A, outer concrete element type: C3D8R B, core concrete element type: C3D8R

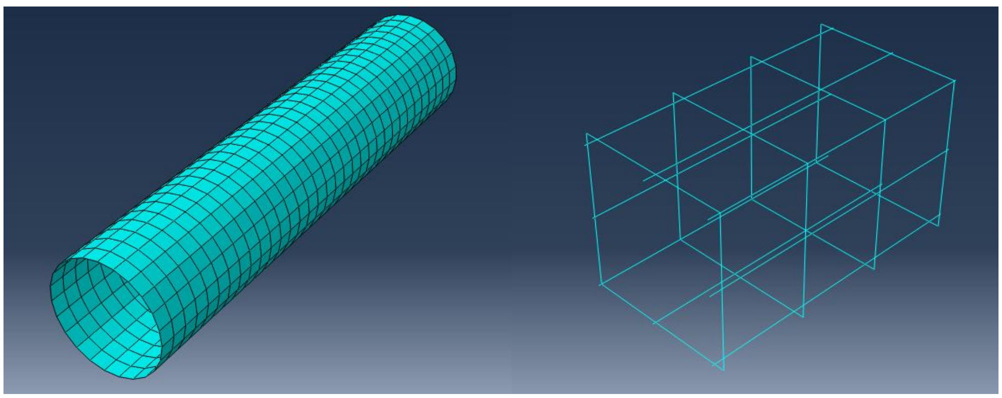

C, steel tube element type: S4R D, Reinforcement bar element type: T3D2

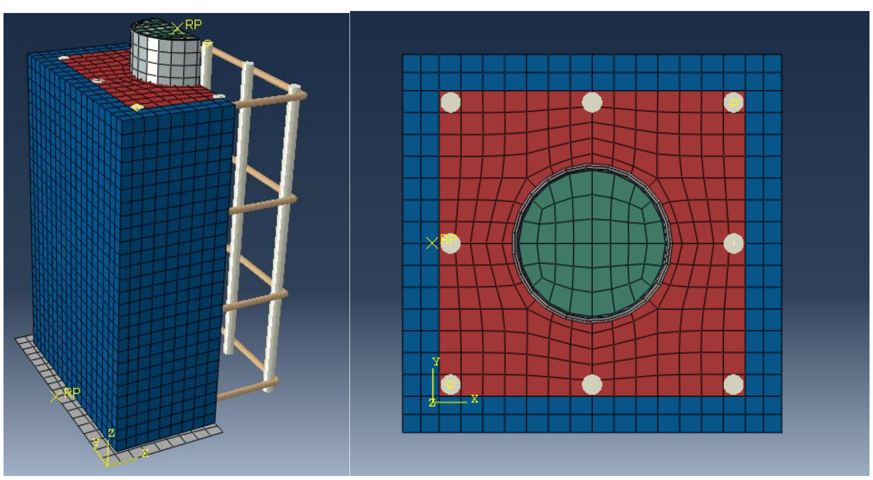

E, overall finite element model

Fig 4. 10 Element types and mesh

4.6 Boundary Condition and Steel-Concrete Interfaces

Each part of the finite element is independently modeled and assembled to the exact place to arrange the sample specimen. The interaction between the outer concrete and rebar (longitudinal and stirrups) were modeled by "embedded constraint" in ABAQUS shown in Fig 4.11B. Rebars are placed in the concrete, which the concrete will consider as the host region, and the reinforcement was embedded. At which the degree of freedom at the node of the bar was restrained. "Tie constraint" is used to model the interaction between the concrete and the rigid plate so that the degree of freedom will be the same during loading. Also, tie constraint interaction is applied between the reinforcement bar and rigid plate, between load plate and CFST surface. In all case the plates considered as master surface and the concrete and steel tube considered as slave surface.

The rigid plate is restrained at the reference point against all rotational and transitional movements to represent the base plate in the push-out experiment shown in Fig 4.11A. Dynamic explicit is applied to create a loading process in Abaqus, which has similar loading to the experimental. Uniform downward displacement applied with smooth step amplitude on the top surface of concrete-filled steel tube at the reference point to create slip between the steel tube and outer concrete as shown in Fig 4.11A.

"General contact" is used to define the interaction behavior between the steel tube and concrete at the interfaces. General contact can be defined by a "hard contact" relationship in the normal direction between the steel tube and concrete. This behavior can be defined by there is no contact pressure unless one surface contacts another. The contact surfaces are allowed to separate each other after they have been contacted. A "Penalty friction" formulation in the tangential direction. The friction coefficient is 0.5 taken from the Coulomb friction model, which gives good agreement to the experimental result. Surface-based cohesive properties defined in general contact behavior discussed in section 4.4. There are two interfaces available in concrete-encased concrete-filled tubes; those are steel tube to core concrete and steel to outer concrete. Nodes on slave surface can not penetrate the master surface. Analytical rigid surfaces always be master surface.

Coulomb friction model suggests that the bond stress is transferred into the surface when the applied bond stress is greater than the critical bond stress. After the development of relative slip between the steel tube and concrete surface, bond stress is equal to critical bond stress. Mathematically expressed by Roeder, Cameron, *et al.*, (1999): $\tau_c \geq \tau_B$

Where, $\tau_c = \mu * F$, F is the applied push load, μ is friction coefficient, τ_c is critical bond stress (N/mm^2), τ_B is average Bond stress of core concrete to steel tube (N/mm^2).

At the interfaces between outer RC and steel tube, average bond strength of 1.78N/mm^2 was used for the shear stress limit of the finite element model. Average bond strength (1.78N/mm^2) was found from the experimental investigation discussed in section 5.2. Generally, the interface behavior between steel and concrete can be defined by general contact behavior. These include hard contact behavior in the normal direction, penalty friction formulation on the tangential direction, and surface-based cohesive property.

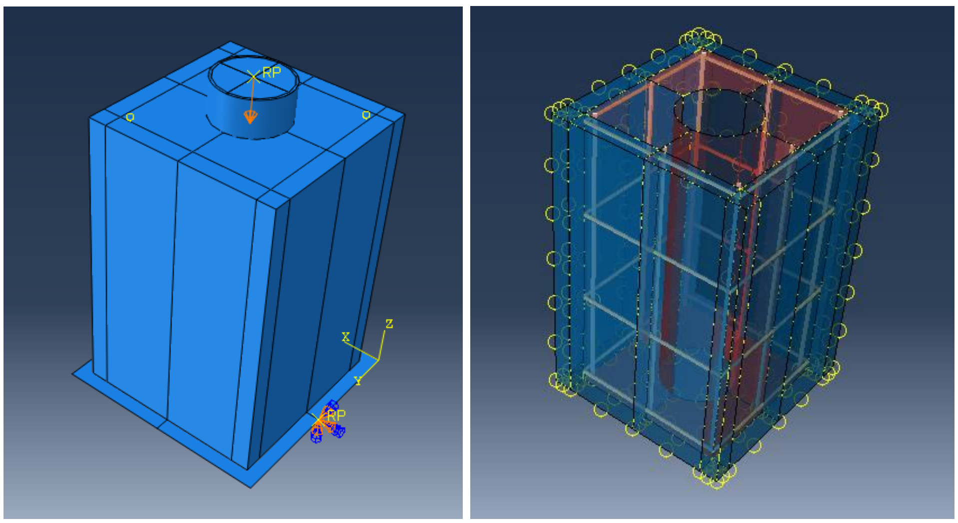

A, rigid constraint at the RP of base plate B, Rebar embedded in concrete

Fig 4. 11 boundary condition and interaction

4.7 Method of Analysis

There are two methods of analysis to investigate the interaction problem in the ABAQUS, those are Abaqus quasi-static analysis and dynamic explicit analysis. The quasi-static method is generally used to predict the unstable and nonlinear collapse of a structure. It is an implicit load control method. In the quasi-static method, the load is applied proportionally in several load steps. In each load step, the equilibrium iteration is performed and the equilibrium path is tracked in the load-displacement space. This method is often used in static analysis and shows to be a strong method for nonlinear analysis. However, due to the equilibrium iteration, the quasi-static method consumes much time and computer resources for a relatively large model. Moreover, the convergence problem is often encountered when material damage and failure are included and thus the ultimate load could not be achieved. In this study, the dynamic explicit analysis method was employed. A dynamic explicit analysis is a time control method. It is popularly used for the problems of impact, metal forming, progressing damage and failure of the material, and so on. It shows to be a powerful solution scheme for discontinuous medium, contact interaction, and large deformation. It has been applied in many problems such as crack and failure of concrete material, metal sheet forming, composite laminate impact, etc. In the dynamic explicit analysis method, the global mass and stiffness matrices need not be formed and inverted so each increment is relatively inexpensive compared to the implicit analysis. The size of the time increment is determined dependent on the mesh size and material properties. An explicit analysis is very efficient for solving discontinuous and contact problems; thus, it is appropriate for push-out test simulation. The dynamic explicit method can be used to simulate a push-out test with the same loading rate as in the real experiment.

CHAPTER 5. RESULTS AND DISCUSSION

5.1 General observation

No damage occurred on the specimens during the test. But there was a slip between the steel tube and outer reinforced concrete. Neither the steel tube buckled nor the concrete crushed was observed during testing. Some debris of concrete appears at the interfaces during the slip of the steel tube to outer RC. The noise was heard at the loading of the test.

5.2 Bond Stress to Slip Curves

In this paper, average bond stress is used to define the bond between the steel tube and outer concrete. Average bond stress defined us a push load divided by the contact interfaces area between steel tube and outer concrete.

$$\tau = \frac{N_{ue}}{\pi * D_s * L_{int}} \quad (5.\ 1)$$

Where N_{ue} is push load applied on top of CFST (loaded end), D_s is diameter of steel tube, and L_{int} is the interface contact length of steel tube and outer concrete which is 400mm for all specimen.

Generally, three type bond stress to slip curve were observed on the experimental investigation of nine specimens shown in Fig 5.1. Each curve type will be discussed as follows.

The first type of curve is the curve A, which shows the linear elastic response from 0 to A, the bond stress to slip curve at point A is 65% to 78% of peak bond strength. Then the curve tends to slightly decrease from point A to B (peak bond strength). After reaching the peak bond strength, the curve rapidly declines from point B to C. Then, the curve tends to increase rapidly from point C to D. The increasing and decreasing slope will continue up to the slip end.

The second type of curve is the curve B, which shows the linear elastic response from 0 to A, the bond stress to slip curve at point A is 54% to 67% of peak bond strength. After that, the curve tends slightly decrease from point A to B (peak bond strength). After reaching the peak bond strength, the curve rapidly declines from point B to C. Then the curve tends to be relatively stable residual bond strength. The bond strength straight or flattens approach from point C to D.

The third type of curve is the curve C. The bond stress to slip curve is characterized by the lacking of any falling branch. Type C curve shows linear elastic up to point A, 73.5% of peak bond stress.

Then there will be decreasing in stiffness up to point B (ultimate bond strength). After reaching point B, the curve continues increasing with an inelastic response up to point C. Each curve shows similar behavior to that of Tao *et al.*, (2011), but in the current investigation the residual bond stress to slip curve shows decreasing and increasing slope, which some specimens show similar behavior to Han *et al.*, (2016).

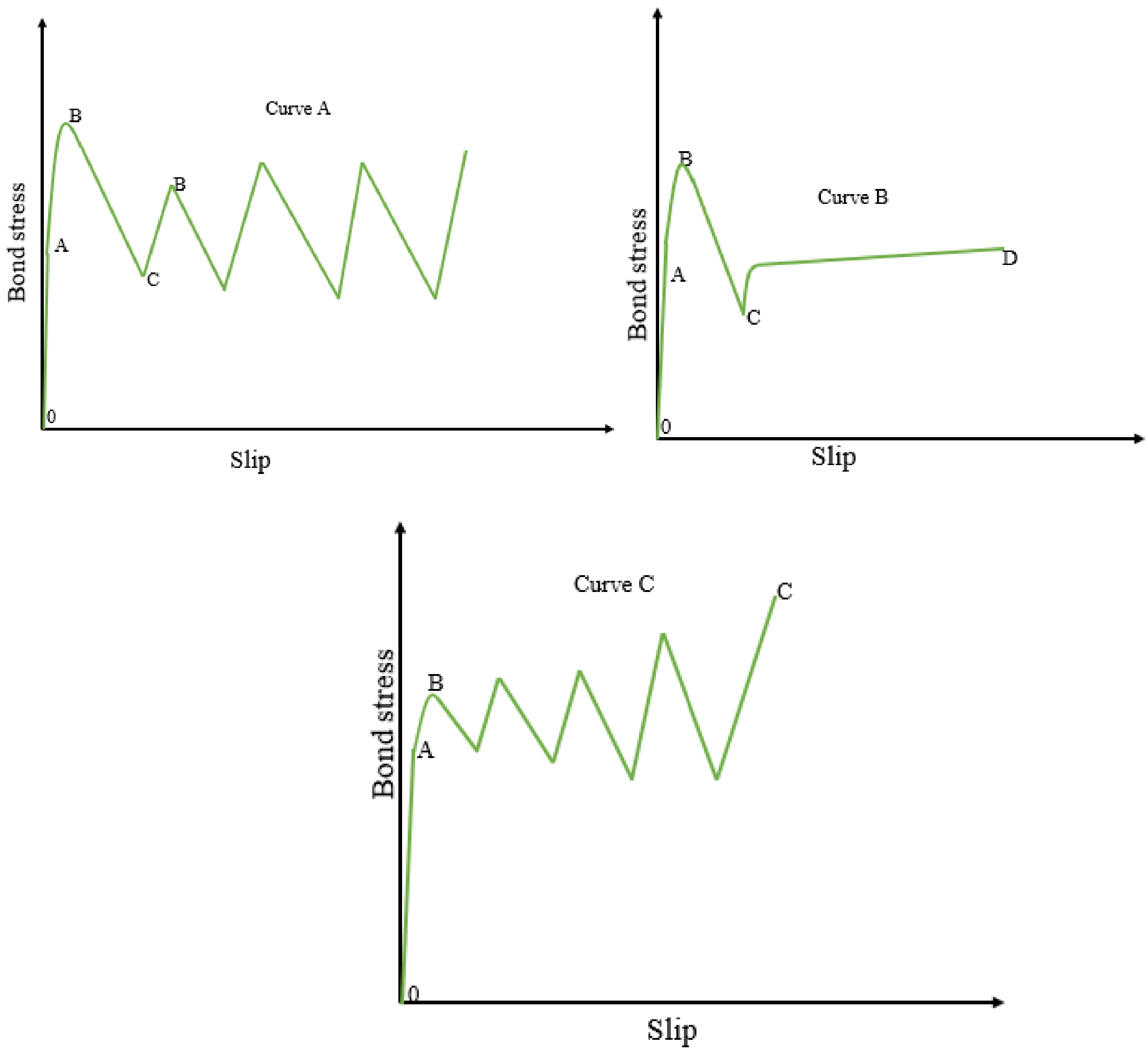

Fig 5. 1 types of bond stress to slip curve

Table 5. 1 summary of the experiment

Specimen label	D*t, (mm*mm)	*concrete strength*, (MPa)	Concrete cover, (mm)	Spacing of stirrups	N_{ue}, (kN)	τ_u, (N/mm^2)	Curve Type
CE-CFST 11	102*3	45	60	Ǿ8 c/c 125mm	277.11	2.16	A
CE-CFST 12	102*3	45	60	Ǿ8 c/c 70mm	288.87	2.25	A
CE-CFST 13	102*3	45	80	Ǿ8 c/c 125mm	265.11	2.07	B
CE-CFST 14	102*3	45	80	Ǿ8 c/c 70mm	294.37	2.3	B
CE-CFST 21	102*3	35	60	Ǿ8 c/c 125mm	156.31	1.21	C
CE-CFST 22	102*3	35	60	Ǿ8 c/c 70mm	172.57	1.35	B
CE-CFST 23	102*3	35	80	Ǿ8 c/c 125mm	225.51	1.76	A
CE-CFST 24	102*3	35	80	Ǿ8 c/c 70mm	260.1	2.03	A
CE-CFST 31	102*3	25	80	Ǿ8 c/c 125mm	254.5	1.99	B

CE-CFST 11

CE-CFST 11 is a composite specimen experimentally conducted with material properties of 45MPa compressive strength, 60mm of concrete cover, and 125mm spacing of transverse reinforcement.

The bond stress to slip curve of CE-CFST 11 is similar to the type A curve discussed in Fig 5.1. The bond stress to slip curve of specimen CE-CFST 11 is shown in Fig 5.2. Bond stress to slip curve starts with a linear relationship up to 65% of the peak bond stress (ultimate bond stress) due to chemical adhesion and steel surface roughness formed between steel tube and concrete interfaces. Then the stiffness of bond stress to slip curve slightly decreased due to loss of chemical adhesion and starting the contribution of mechanical interlock. The bond stress reached peak bond stress when the slip travel 2.01mm. After reaching the peak point (2.16 N/mm^2 or 277.1kN from data logger), the bond stress to slip curve rapidly decline (sudden load drop) up to 0.14 N/mm^2, because of loss of chemical adhesion and mechanical interlock. After the rapid decline of the bond stress to slip curve, the bond stress increases linearly due to reactivation of mechanical interlock (steel surface roughness and irregularity of steel tube). The increasing and decreasing of bond stress to slip curve continues up to the slip end.

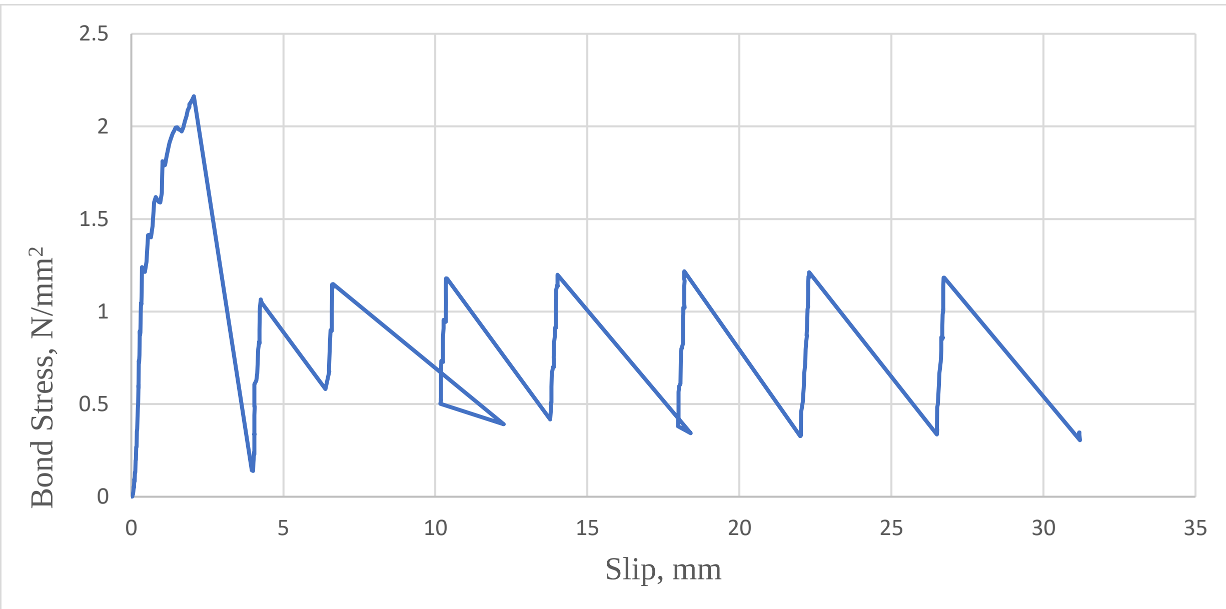

Fig 5. 2 Bond stress to slip curve of CE-CFST 11

When the bond stress reaches the peak point a heavy noise is heard and the bond stress decline with a steep slope to 0.14N/mm^2. After the decline, the bond stress increases linearly up to 1.07N/mm^2, and heavy noise is heard again. Then the bond stress declined to 0.58N/mm^2. This loading process continues up to the final slip shown in Fig 5.2. Post experimental investigation revealed that the heavy noise emanated from the separation of chemical adhesion and mechanical interlock (steel surface roughness and steel surface irregularity) between the steel tube and outer concrete interfaces.

Fig 5. 3 view of specimen after testing

The bond resistance of concrete-encased concrete-filled steel tubes originated from three composite actions; chemical adhesion, micro-interlock (steel surface roughness), and macro-interlock (steel tube irregularity). Friction marks were observed evenly distributed throughout the outer surface of the steel tube, which indicates that the slip at the interfaces was resisted by the whole steel surface or have a contribution to bond strength is shown in Fig 5.4. No visible damage or cracks formed in the outer concrete due to the strain on the outer concrete was less than 300με throughout the loading process, but the cracking strain of concrete was 350 με. This implies that the concrete remains in the elastic range on the loading process. The longitudinal strain and hoop strain at different loading processes was recorded by three strain gauges installed along the length.

In this paper, the first peak bond stress or ultimate bond stress between steel tube and outer concrete interfaces represent the bond strength of CE-CFST 11. Which is 2.16N/mm^2 used for bond capacity. Eurocode 4.1, (2004) and ES-EN1994:(2015) recommended the bond strength of concrete-encased steel-concrete structure should be larger than 0.4N/mm^2 and 0.5N/mm^2. The bond strength of the steel tube to outer concrete found from the experiment satisfied the requirement.

Fig 5. 4 Friction resistance of steel tube at the interfaces

The residual bond strength for this specimen taken us the maximum bond stress after ultimate bond stress is 1.22N/mm^2. The chemical adhesion is only active up to the first part of the elastic range. After that, the bond resistance mainly arises from micro interlocking and macro interlocking. The contribution of micro interlock gradually decreases and residual bond resistance mainly comes from macro interlock.

CE-CFST 12

CE-CFST 12 is a composite specimen experimentally conducted with material properties of 45MPa compressive strength, 60mm of concrete cover, and 70mm spacing of transverse reinforcement.

The bond stress to slip curve of CE-CFST 12 is similar to the type A curve discussed in Fig 5.1. The average bond stress to slip curve of CE-CFST 12 is similar to CE-CFST 11 except the bond stress to slip curve of CE-CFST 12 is stiffer up to ultimate bond strength shown in Fig 5.5. The bond stress continues linearly up to 78% of ultimate bond stress (1.76N/mm^2). The stiffness decreases and ultimate bond stress is achieved at 2.25N/mm^2. The bond stress reached peak bond stress when the slip travel 1.72mm. There was a sudden load drop up to 0.55N/mm^2 and reactivation of bond stress up to 1.05N/mm^2. The bond stress to slip curve continues with sudden load drop due to loss of macro interlock and rise of load due to reactivation of macro interlock up to slip of 20mm.

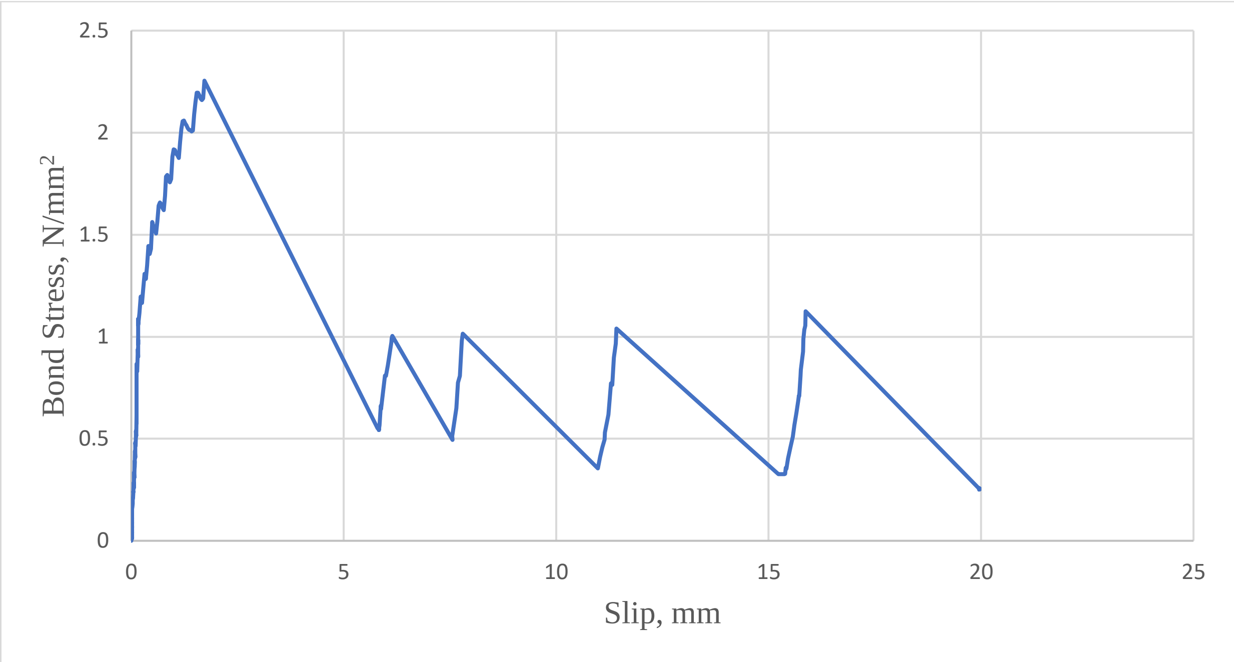

Fig 5. 5 Bond Stress to Slip Curve of CE-CFST 12

Heavy noise was heard when the composite action between steel tube and concrete lost their bond at the interfaces. Friction marks were evenly distributed in steel tube surfaces. No visible damage or cracks formed in outer concrete as shown in Fig 5.6. No buckling of the steel tube was observed.

Fig 5. 6 view of specimen after testing

The bond strength of CE-CFST 12 is 2.25N/mm^2, which is the ultimate bond stress. The residual bond strength of CE-CFST 12 is higher than that of CE-CFST 11. The residual bond strength for CE-CFST 12 is 1.12N/mm^2. The reason is that, the confinement of concrete increased by a close arrangement of transverse reinforcement (70mm c/c Ǿ8mm).

CE-CFST 13

CE-CFST 13 is a composite specimen experimentally conducted with material properties of 45MPa compressive strength, 80mm of concrete cover, and 125mm spacing of transverse reinforcement.

The bond stress to slip curve of CE-CFST 13 is similar to the type B curve discussed in Fig 5.1. The bond stress to slip curve of CE-CFST 13 starts with linear part up to 1.38N/mm^2 (66% of peak bond stress) followed by a decrease in stiffness up to 2.07N/mm^2 or 265kN from the data logger (peak bond stress) shown in Fig 5.7. After the peak bond stress, sudden load drops appear up to 0.18N/mm^2 or 23.26kN from the data logger. The bond stress reached peak bond stress when the slip travel 2.18mm. The residual bond stress to slip curves of CE-CFST 13 was relatively horizontal up to slip ends. The residual bond stress values continue with the minimum residual bond strength of 0.18N/mm^2 and maximum residual bond strength of 1.1N/mm^2 up to the end of the slip (38mm) travel limit, which is 1.07N/mm^2 (51.7% peak bond stress).

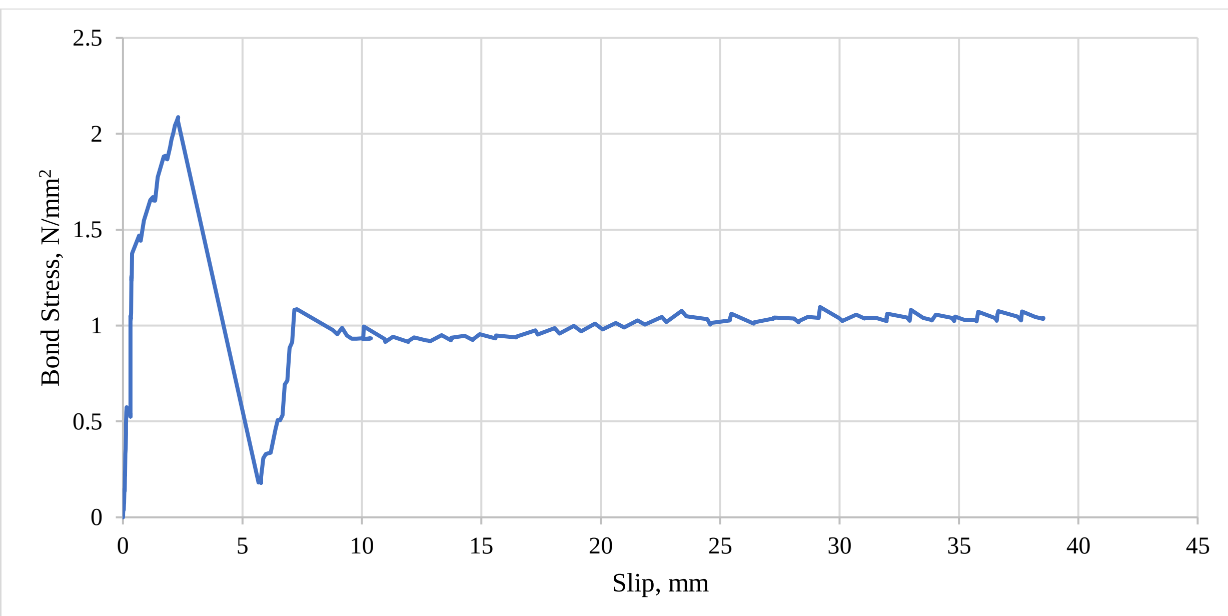

Fig 5. 7 Bond Stress to Slip Curve of CE-CFST 13

Heavy noise was heard only when the steel tube and concrete at the interfaces lost their bond at peak bond stress. Friction marks were evenly distributed on steel tube surfaces. No visible damage or cracks formed in outer concrete, but the crack was formed on the bottom surface of the concrete (at the free end load), which started from the outer surface of the steel tube, but it did not continue to the edge of the concrete shown in Fig 5.8. No buckling of the steel tube was observed.

Fig 5. 8 view of specimen after testing

The bond strength of specimen with type B curve is straightforwardly taken as peak bond stress (2.07N/mm^2) of the average bond stress to slip curve. The average bond stress to slip curve of the specimen remain slightly horizontal after a sudden load drop and continues the slip up to the travel limit. So that, the residual bond strength is simply taken as 1.1N/mm^2.

CE-CFST 14

CE-CFST 14 is a composite specimen experimentally conducted with material properties of 45MPa compressive strength, 80mm of concrete cover, and 70mm spacing of transverse reinforcement.

The bond stress to slip curve of CE-CFST 14 is similar to the type B curve discussed in Fig 5.1. The bond stress to slip curve of CE-CFST 14 starts with linear part up to 1.25N/mm^2 (54% of peak bond stress) followed by a decrease in stiffness up to 2.3N/mm^2 or 294.5kN from the data logger (peak bond stress) shown in Fig 5.9. After the peak bond stress, sudden load drops down appear up to 0.18N/mm^2 or 23.26kN from the data logger. The bond stress reached peak bond stress when the slip travel 1.13mm. The residual bond stress to slip curves of CE-CFST 14 was relatively horizontal up to slip ends. The residual bond stress values continue with the minimum residual bond strength of 0.2N/mm^2 and maximum residual bond strength of 1.13N/mm^2 up to the end of the slip (38mm) travel limit, which is 1.13N/mm^2 (49.13% peak bond stress).

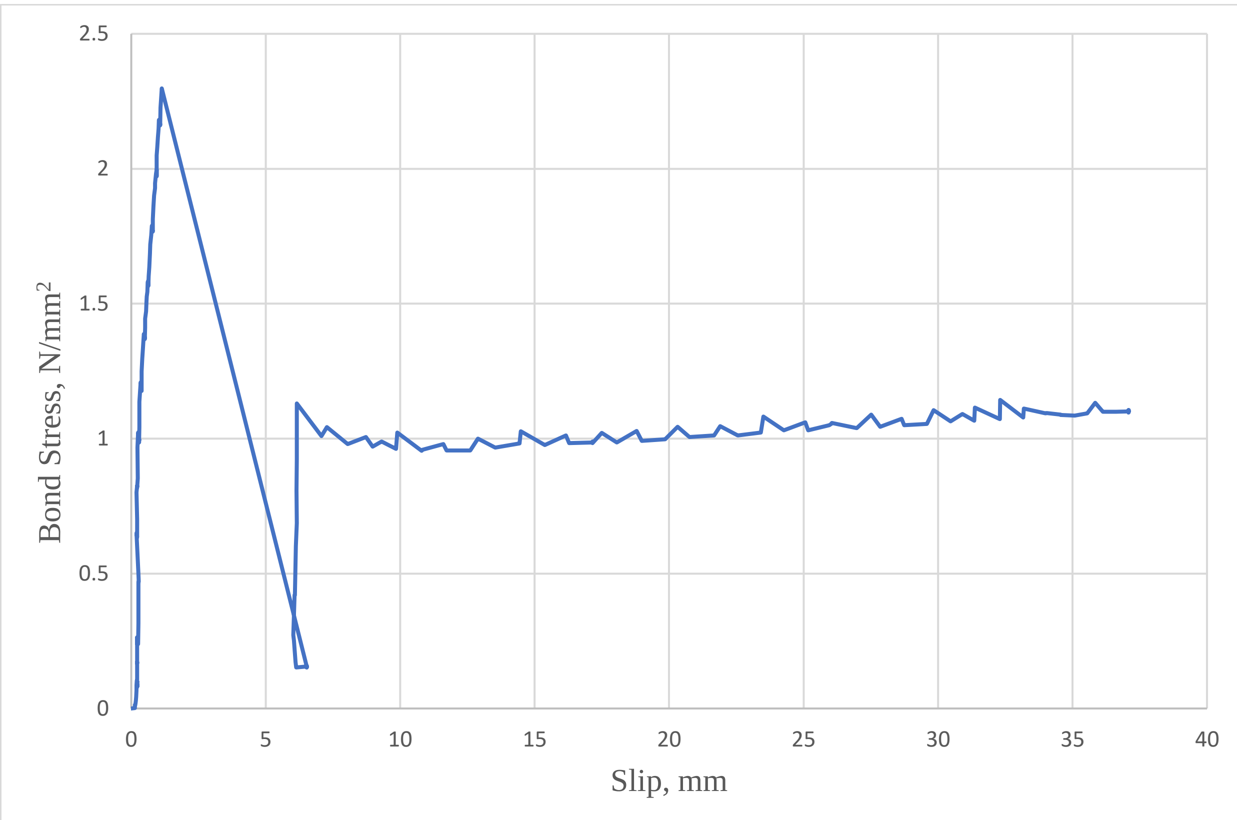

Fig 5. 9 Bond Stress to Slip Curve of CE-CFST 14

Heavy noise was heard only when the steel tube and concrete at the interfaces lost their bond at peak bond stress. Friction marks were evenly distributed in steel tube surfaces. No visible damage or cracks formed in outer concrete, but minor crack was formed on the bottom surface of the concrete (at the free end load) which started from the outer surface of the steel tube, but it did not continue to the edge of the concrete as shown in Fig 5.10. No buckling of the steel tube was observed.

Fig 5. 10 view of specimen after testing

The bond strength of specimen with type B curve, the bond strength is straightforwardly taken as peak bond stress (2.3N/mm^2) of the average bond stress to slip curve. The average bond stress to slip curve of the specimen remain slightly horizontal after a sudden load drop, and continues the slip up to the travel limit. So that the residual bond strength is simply taken as 1.13N/mm^2.

CE-CFST 21

CE-CFST 21 is a composite specimen experimentally conducted with material properties of 35MPa compressive strength, 60mm of concrete cover, and 125mm spacing of transverse reinforcement.

Type C bond stress to slip curve is shown in Fig 5.11 for CE-CFST 21. Type C shows the bond stress to slip curve after linear part is increasing without a falling branch. This type of bond stress to slip curve is shown for this specimen only. At the first stage, there is a linear response up to 0.89N/mm^2, which is 73.5% of the ultimate bond stress. Then the stiffness decreases and the first peak bond stress reached 1.21N/mm^2, the bond stress reached peak bond stress when the slip travel 1.68mm. After the peak point, the bond stress decreased to 1.05N/mm^2 due to loss of micro interlock. The bond stress recovered and increased up to the ultimate bond strength of 1.46N/mm^2 shown in Fig 5.11. The bond stress increases linearly due to reactivation of mechanical interlock (steel surface roughness and irregularity of steel tube). The increasing and decreasing of bond stress to slip curve continues up to the slip end.

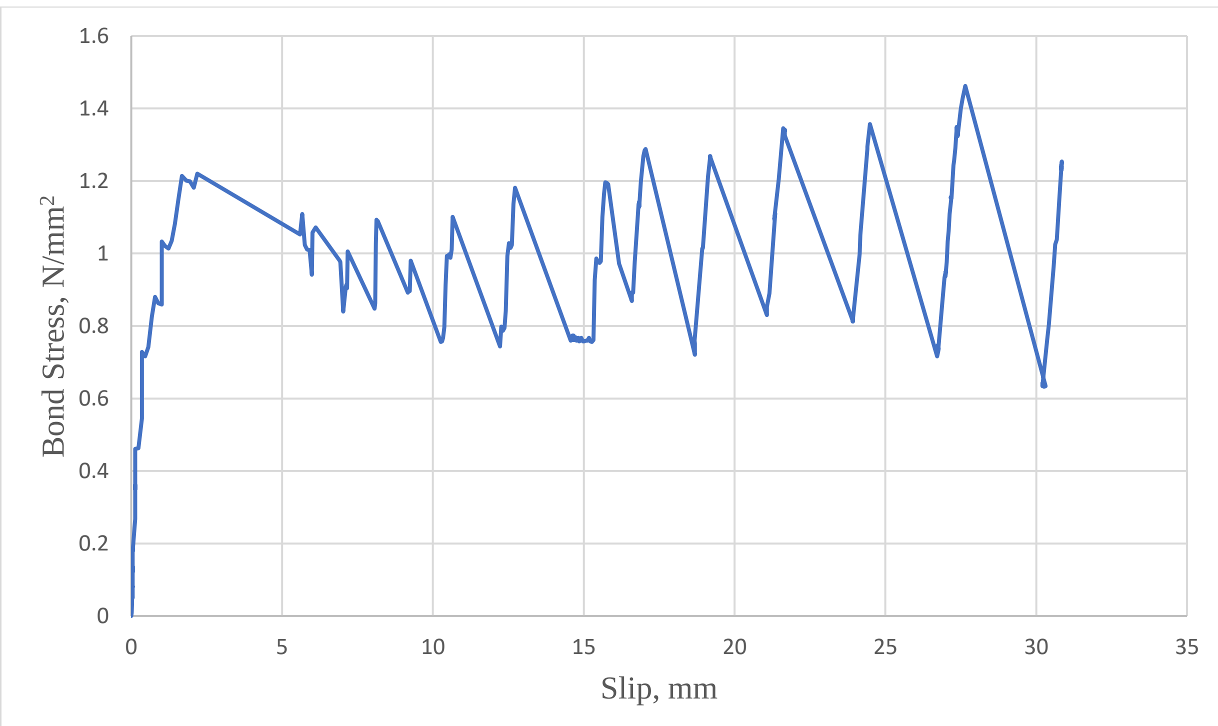

Fig 5. 11 Bond stress to slip curve CE-CFST 21

Some noise could be heard repeatedly during the loading process. But heavy noise was heard after the linear portion. Post experimental investigation revealed that the increase of noise after linear part is due to increases of bond resistance that come from macro interlock or surface irregularity, which increases the applied push load from 156.31kN (1.21N/mm^2) to 187.04kN (1.46N/mm^2) from the data logger.

The bond strength definition is not straight forward for the type C curve because the bond stress increases up to slip travel limit, so the transitional point from the end of decreasing stiffness and the start of the loss of chemical adhesion taken as the ultimate bond strength by Tao *et al.*, (2011), K.S. Virdi and P.J. Dowling, (1980). However, the bond stress to slip curve of CE-CFST 21 is straight forward to identify the first peak bond stress or translation point. So that 1.21N/mm^2 is taken as the ultimate bond strength.

The residual bond strength is taken as the maximum bond stress (1.46N/mm^2) after the peak bond stress. For the current specimen, the residual bond strength is 20% greater than the ultimate bond strength.

CE-CFST 22

CE-CFST 22 is a composite specimen experimentally conducted with material properties of 35MPa compressive strength, 60mm of concrete cover, and 70mm spacing of transverse reinforcement.

The bond stress to slip curve of CE-CFST 22 show similar behavior with the type B curve. With maximum bond stress of 1.35N/mm^2 or 172.6kN from the data logger. The bond stress reached peak bond stress when the slip travel 1.42mm. The residual bond stress is 1.1N/mm^2. The bond strength is taken as maximum bond stress (1.35N/mm^2) shown in Fig 5.12.

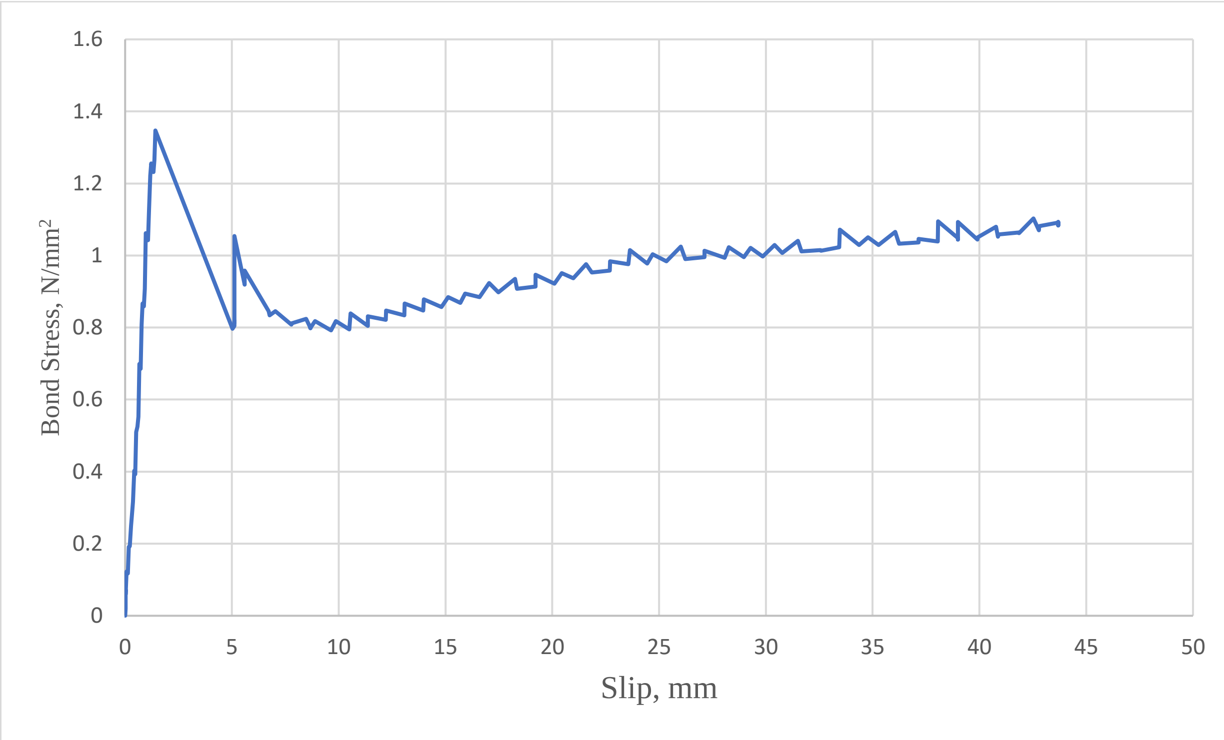

Fig 5. 12 Bond Stress to Slip Curve of CE-CFST 22

CE-CFST 23

CE-CFST 23 is a composite specimen experimentally conducted with material properties of 35MPa compressive strength, 80mm of concrete cover, and 125mm spacing of transverse reinforcement.

The bond stress to slip curve of CE-CFST 23 has similar behavior to CE-CFST 11 and CE-CFST 12. But the peak bond stress of CE-CFST 23 has reduced significantly to 1.76N/mm^2 at a slip of 1.57mm travel limit. The linear portion continues up to 66.4% of the peak bond stress. After that, the bond stress suddenly drops to 0.25N/mm^2 then the bond stress increases linearly up to 1N/mm^2. The ascending and descending part of bond stress to slip curves continue up to the travel limit shown in Fig 5.13.

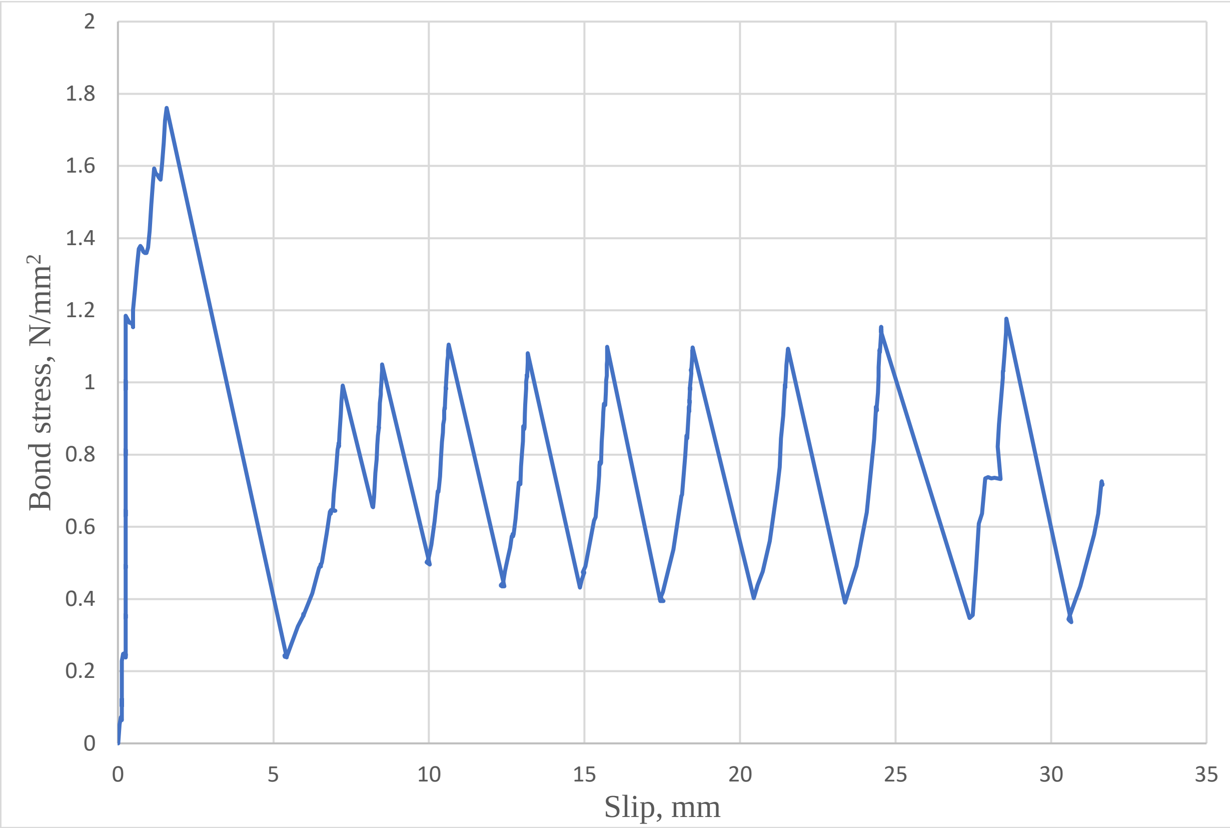

Fig 5. 13 Bond Stress to Slip Curve of CE-CFST 23

The peak bond stress is taken as the bond strength of CE-CFST 23. Which have similar behavior to the first two specimens (CE-CFST 11 and CE-CFST 12). The residual bond strength is taken as the maximum bond stress after the peak bond stress.

CE-CFST 24

CE-CFST 24 is a composite specimen experimentally conducted with material properties of 35MPa compressive strength, 80mm of concrete cover, and 70mm spacing of transverse reinforcement.

The bond stress to slip curve of CE-CFST 24 has similar behavior to CE-CFST 11, CE-CFST 12 and CE-CFST 23. But the peak bond stress of CE-CFST 12 has reduced significantly to 2.03N/mm^2 at a slip of 1.34mm travel limit. The linear portion continues up to 71.9% of the peak bond stress. After that, the bond stress suddenly drops to 0.4N/mm^2 then the bond stress increases linearly up to 1.1N/mm^2. The ascending and descending part of bond stress to slip curves continue up to the travel limit shown in Fig 5.14.

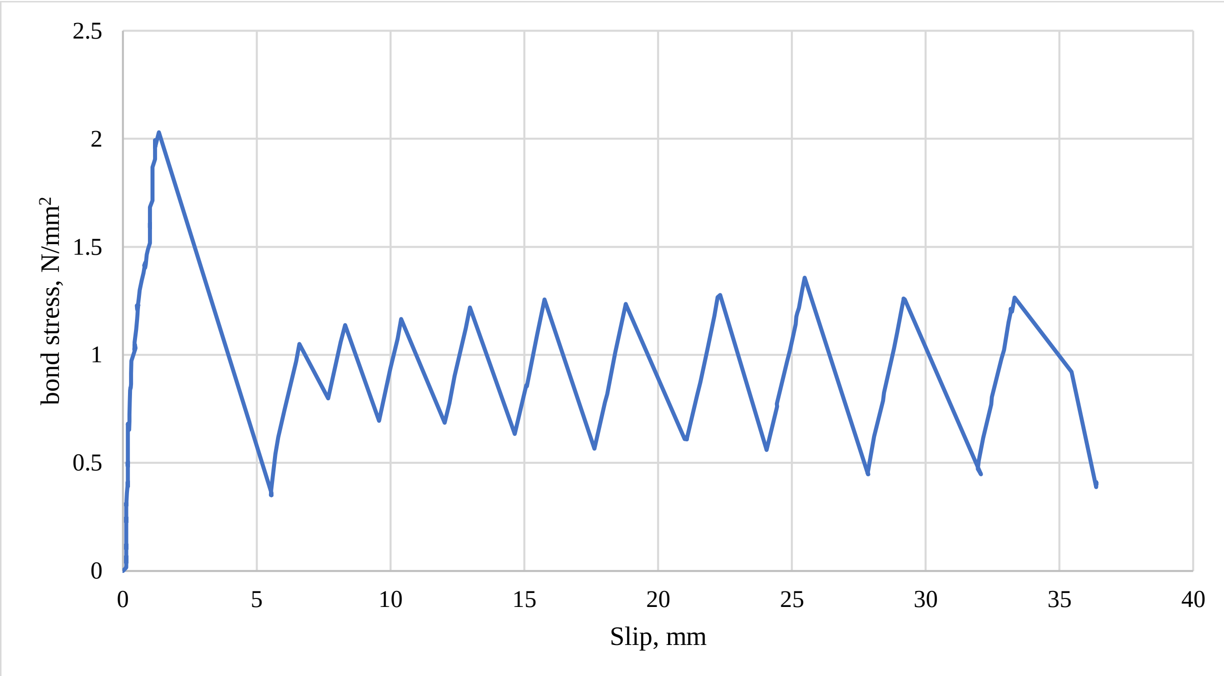

Fig 5. 14 Bond Stress to Slip Curve of CE-CFST 24

The peak bond stress is taken as the bond strength for CE-CFST 24. Which have similar behavior to the first three specimens (CE-CFST 11, CE-CFST 12 and CE-CFST 23). The residual bond strength is taken as the maximum bond stress (1.36N/mm^2) after the peak bond stress. For the current specimen the residual bond strength is 67% of the ultimate bond strength.

CE-CFST 31

CE-CFST 31 is a composite specimen experimentally conducted with material properties of 45MPa compressive strength, 80mm of concrete cover, and 70mm spacing of transverse reinforcement.

The bond stress to slip curve of CE-CFST 31 show similar behavior with the type B curve. With maximum bond stress of 1.9N/mm^2 or 254kN from the data logger. The bond stress reached peak bond stress when the slip travel 1.53mm. The residual bond stress is 1.2N/mm^2. The bond strength is taken as maximum bond stress shown in Fig 5.15.

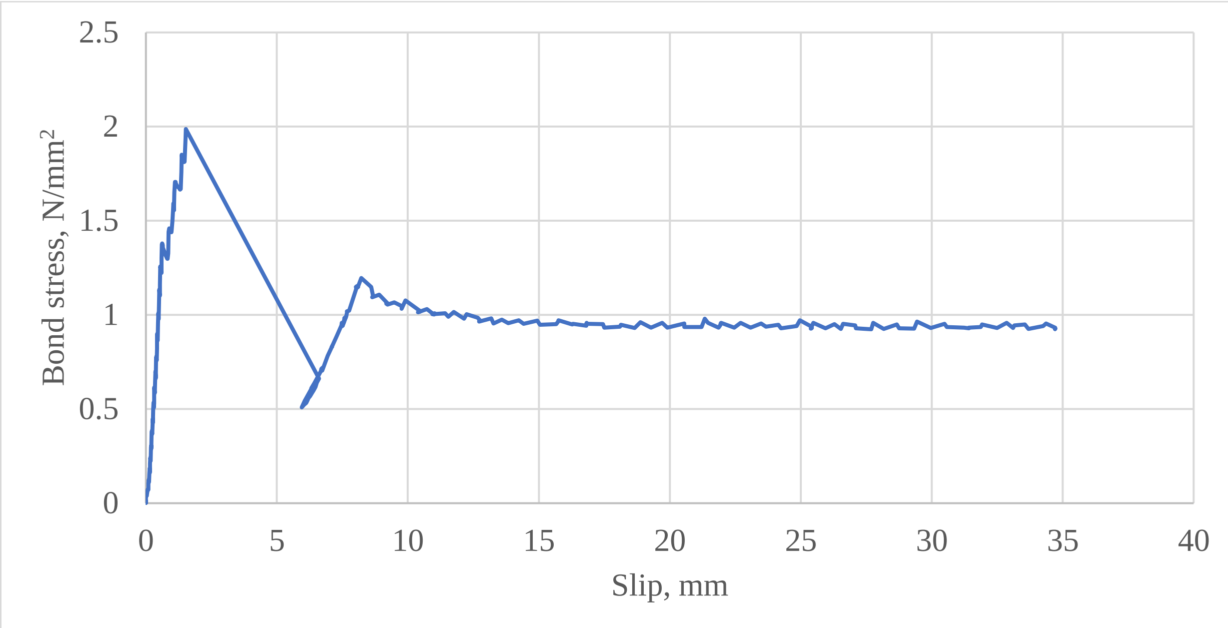

Fig 5. 15 Bond stress to slip curve CE-CFST 31

Numerous researcher have been investigated the bond performance of steel to core concrete interfaces of concrete-filled steel tube. K.S. Virdi and P.J. Dowling, (1980) conducted a push-out test to investigate the bond strength between steel tubes and core concrete. The measured values vary from 0.64MPa to 2.85MPa. Roeder, Cameron, *et al.*, (1999) conducted a push-out test on 18 CFST specimens with measured values ranges from 1.45MPa to 3.29MP*a*. Tao *et al.*, (2011) investigated the bond strength of CFST specimens and found results that vary from 0.15MPa to 0.79MPa. Han *et al.*, (2016) conducted a push-out test for outer concrete and steel tube, found that the bond strength of steel tubes to outer concrete is vary from 2.96 to 4.44MPa with mean values of 3.63MPa. Li *et al.*, (2020) investigated the interaction between steel and concrete by conducting a push-out test on CFDST. The measured values vary from 0.55 to 2.81MPa and 0.57 to 2.61MPa with the mean bond strength of 1MPa and 1.48MPa for outer steel tube to concrete and inner steel tube to concrete interfaces, respectively.

In these experiments, the bond strength varies from 1.18MPa to 2.3MPa with, mean bond strength of 1.78MPa, which is much less than the test made by Han *et al.*, (2016) and greater than the investigation of CFDST of outer interfaces by Li *et al.*, (2020). Between the steel tube and outer concrete interfaces, average bond strength of 1.78MPa was found from the experimental result and used for shear stress limit in the finite element analysis of concrete-encased concrete-filled steel tube members.

5.3 Strain Distribution on Outer Concrete

The strain on the outer concrete surface along the length in the axial and hoop direction was recorded to investigate strain distribution and load transfer mechanism. Axial strain and hoop strain at ultimate load, 75% of ultimate load, 50% of ultimate load, 25% of ultimate load, and post push load were presented to analyze the bond at the interfaces. The negative value was recorded along the length for axial strain while the positive value was recorded for hoop strain.

The longitudinal strain on the outer concrete surface increases from the loading end to the free end. The reason is that the CFST at the loading end is subjected to compression load at the top. When the CFST subjected to compression load, the CFST component laterally expanded at the top of the interfaces because of Poisson, which result in increases of the contact pressure. Because of this, high axial stress-induced in steel tube and low axial stress-induced in outer reinforced concrete, the stress transfer from CFST to outer RC at the top interfaces was not developed. Because of this, the longitudinal strain of outer concrete at the top is small shown in Fig 5.16. From loading end to free end, the compressive stress transferred from CFST to outer RC. The outer RC is subjected to high compressive stress and low compressive stress on CFST due to Poisson effect at the bottom of CE-CFST. But the lateral expansion of outer RC resulted in the separation of CFST from outer RC. Which results in gap formation at the bottom of interfaces shown in Fig 5.17.

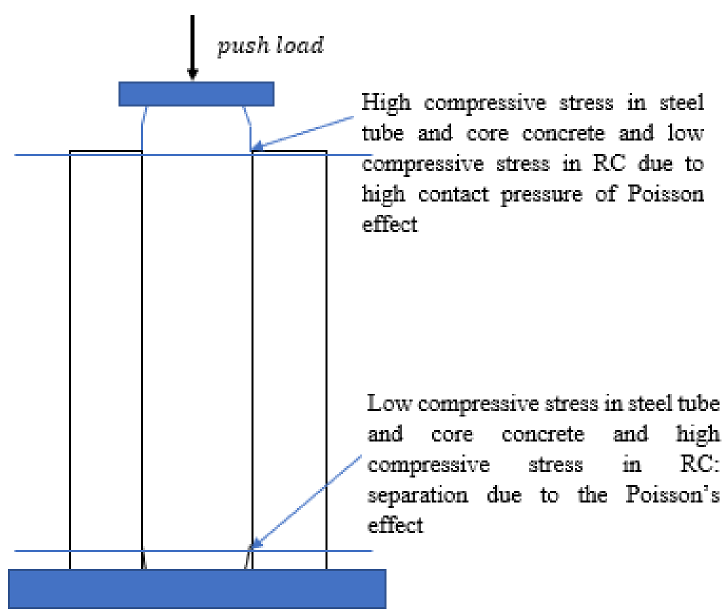

Fig 5. 16 Bond strength mechanism

Fig 5. 17 Gap formation on the free end of the interfaces

In general, maximum hoop strain is achieved at the loading end and decreases to the free end, the reason is the confinement effect at the loading end is high. The hoop strain is positive due to the expansion of concrete in the transverese direction.

The longitudinal strain of outer concrete linearly increases from the loading end to the free end shown in Fig 5.18. This indicates that the push load was transferred from the CFST to the outer RC through the bond stress. Finally, the push load was transferred to the outer RC and into the base plate placed at the bottom of the specimens or ground.

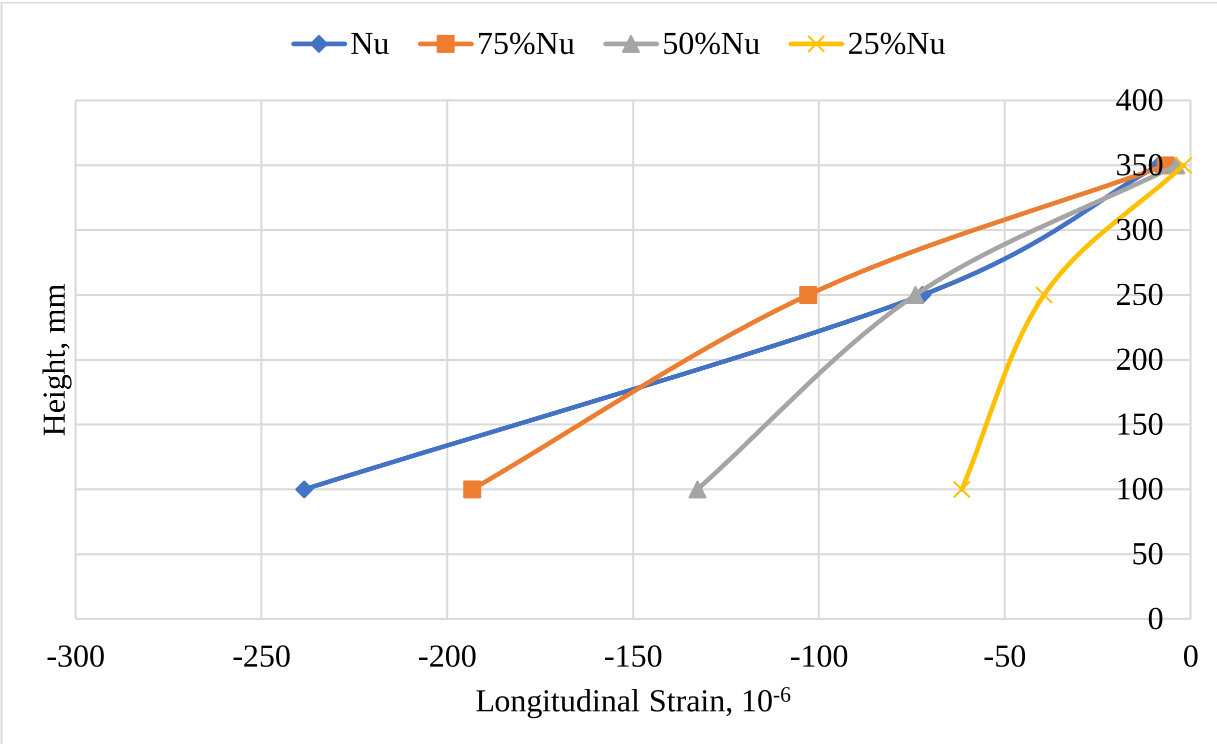

a) Strain Distribution on CE-CFST 11

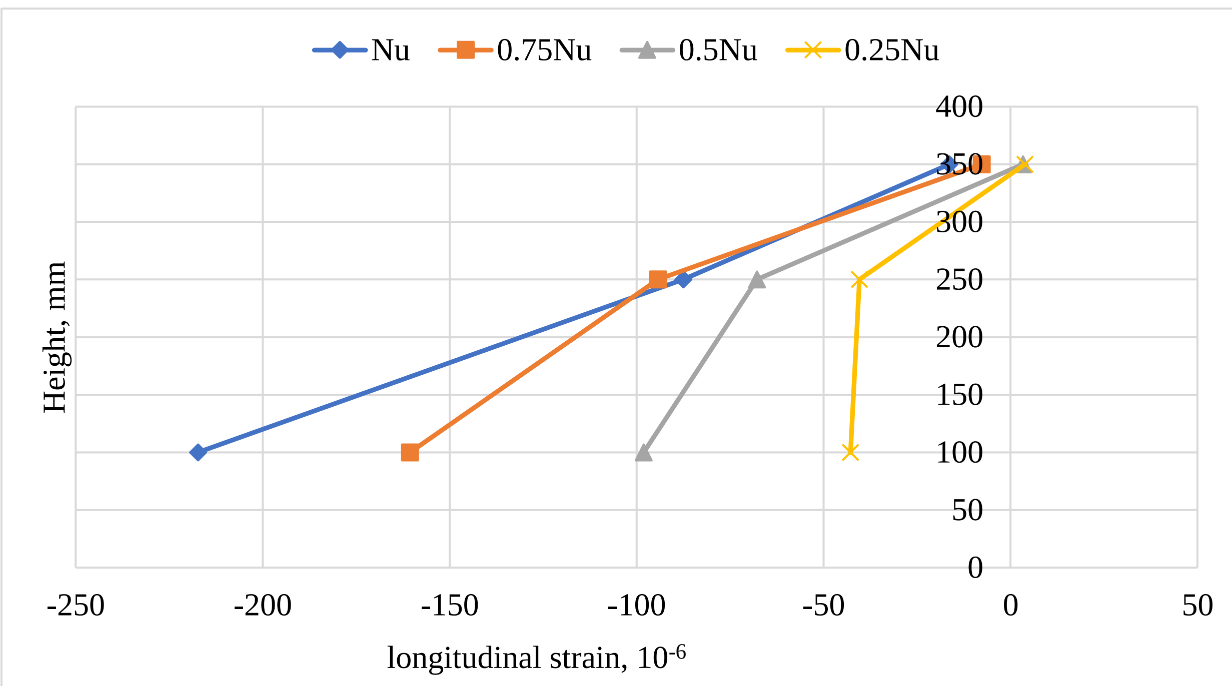

b) Strain Distribution on CE-CFST 12

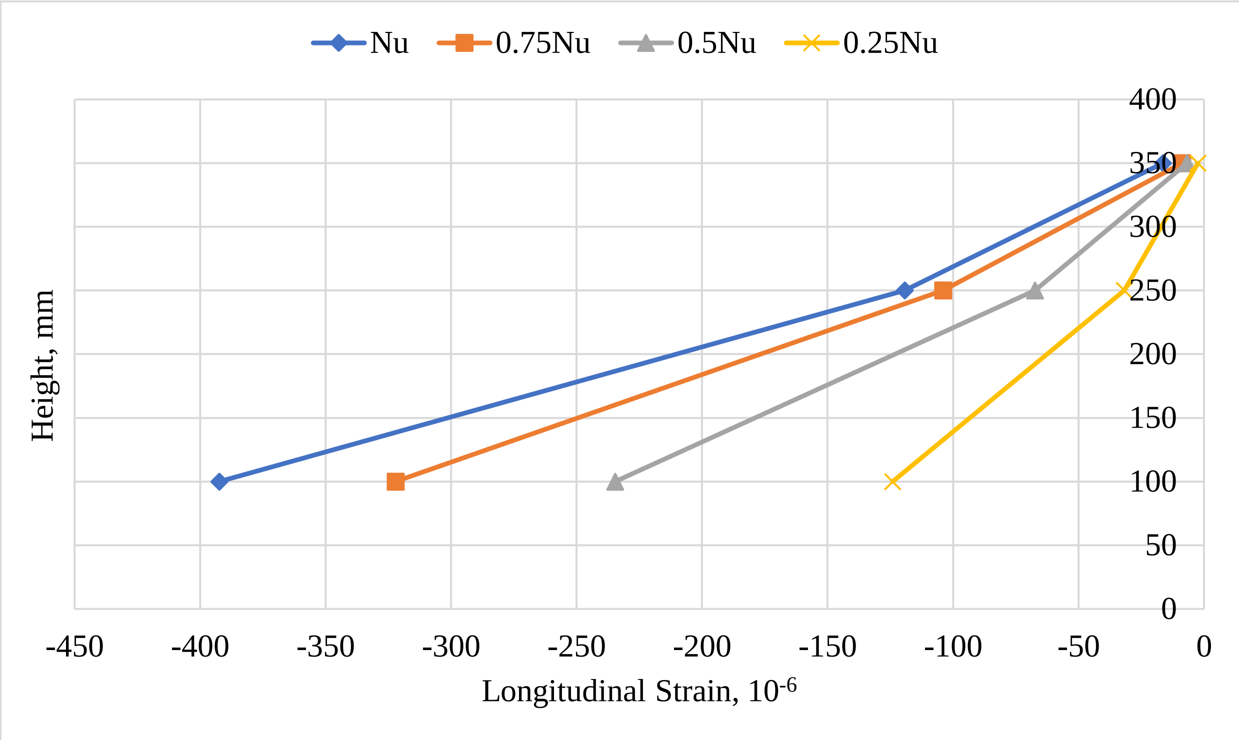

c) Strain Distribution on CE-CFST 14

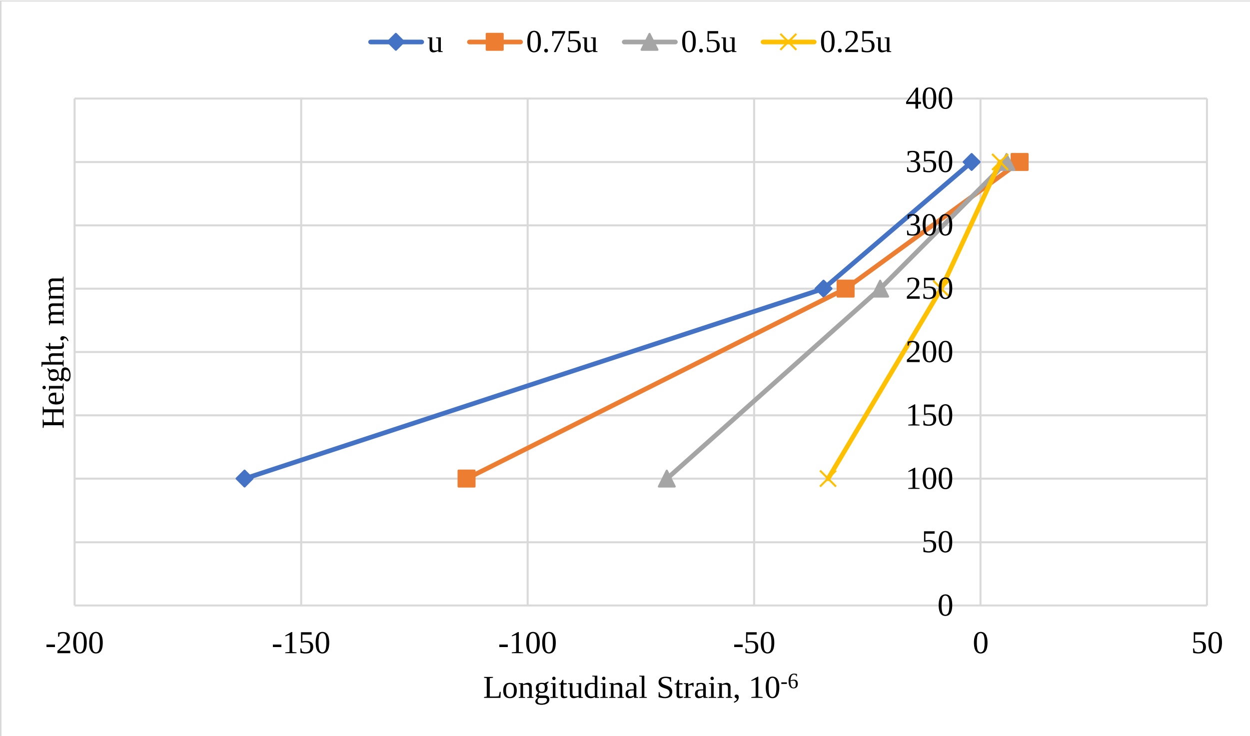

d) Strain Distribution on CE-CFST 22

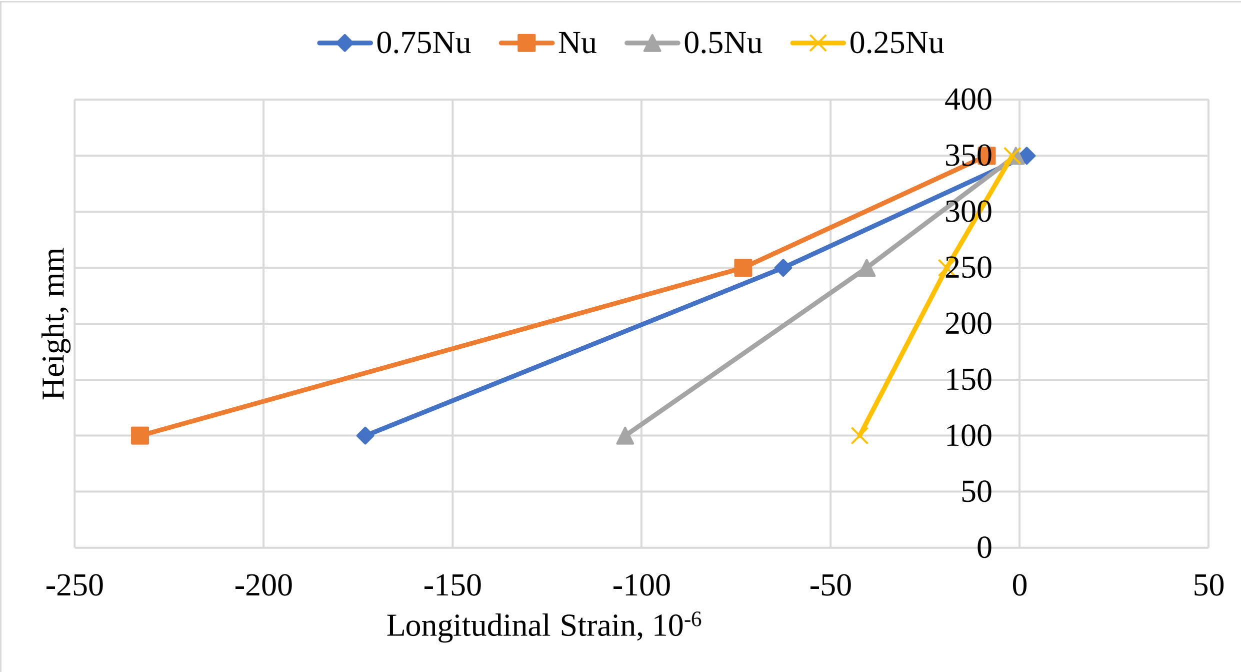

e) Strain Distribution on CE-CFST 23

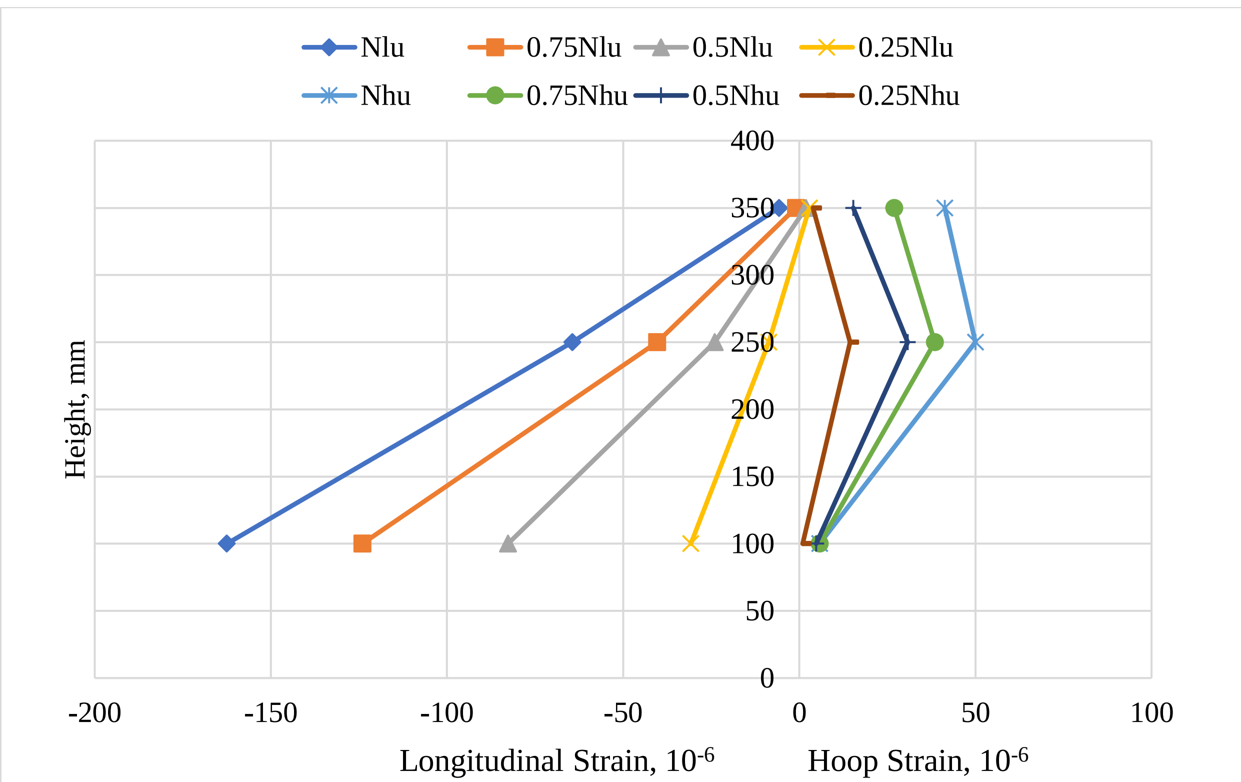

f) Strain Distribution on CE-CFST 24

Fig 5. 18 Distribution of strain along the height of outer concrete external surface

5.4 Influences of various parameters on bond strength

5.4.1 Concrete Strength

The bond strength increases with increases in concrete compressive strength. The reason is that, for high concrete compressive strength, the shrinkage of concrete also increases. This is attributed to the fact that with increasing concrete strength the potential for autogenous shrinkage also increases. Which results in the development of compression in the normal direction of the outer steel tube and potentially better keying action.

The variation of average bond stress with concrete compressive strength is shown in Fig 5.19. From Fig 5.19 it may be seen that the compressive strength has a significant influence on the bond stress. For 60mm concrete cover and 125mm spacing of transverse reinforcement, the average maximum bond stress of CE-CFST 11(2.25N/mm^2) compared to that of CE-CFST 21(1.18 N/mm^2) was 47.5% greater. For 60mm concrete cover and 70mm spacing of transverse reinforcement, the average maximum bond stress of CE-CFST 12(2.16N/mm^2) compared to that of CE-CFST 22(1.35 N/mm^2) was 37.5% greater, shown in Fig 5.19.

For 80mm concrete cover and 125mm spacing of transverse reinforcement, the average maximum bond stress of CE-CFST 13(2.07N/mm^2) compared to that of CE-CFST 23(1.76 N/mm^2) was 18% greater. For 80mm concrete cover and 70mm spacing of transverse reinforcement, the average maximum bond stress of CE-CFST 14(2.3N/mm^2) compared to that of CE-CFST 24(2.03 N/mm^2) was 11.7% greater.

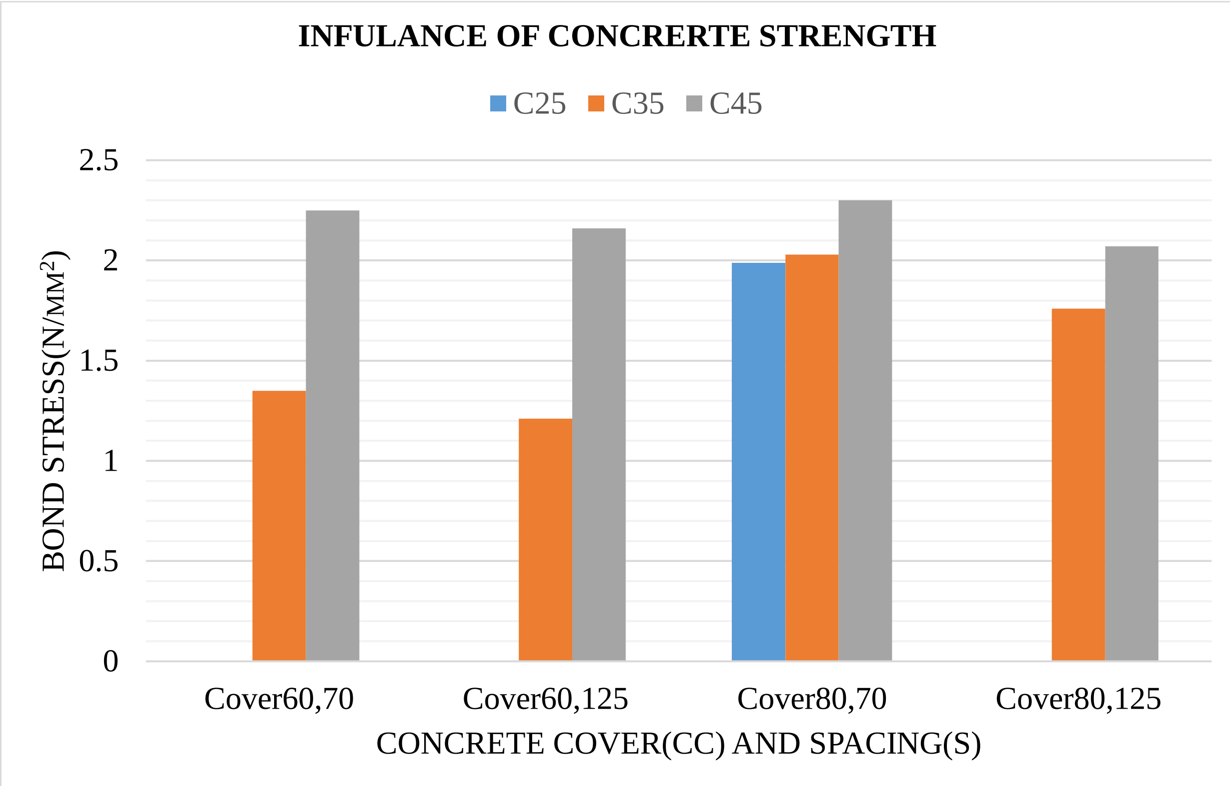

Fig 5. 19 Effect of Concrete strength

5.4.2 Concrete Cover

For the current test, the concrete compressive strength of four specimens is 35MPa. The average maximum bond stress of CE-CFST 21 (1.18N/mm^2) and CE-CFST 22 (1.35N/mm^2) compared to that of CE-CFST 23 (1.76N/mm^2) was 32.95% and CE-CFST 24 (2.03N/mm^2) was 33.5%, respectively, greater, shown in Fig 5.20. The bond stress will increase for larger concrete cover due to the restriction of concrete encasement to lateral deformation.

For the current test, the concrete compressive strength of four specimens is 45MPa. The concrete cover from outer steel surface to outer concrete cover is varied from 60mm to 80mm. The average maximum bond stress is increased from 2.16N/mm^2 to 2.3 N/mm^2 for CECFST 12 and CECFST 14, respectively, which is 8.7% increases in the average maximum bond stress. The average maximum bond stress of CE-CFST 11(2.25N/mm^2) compared to that of CE-CFST 13(2.07N/mm^2) was 8% greater, shown in Fig 5.20.

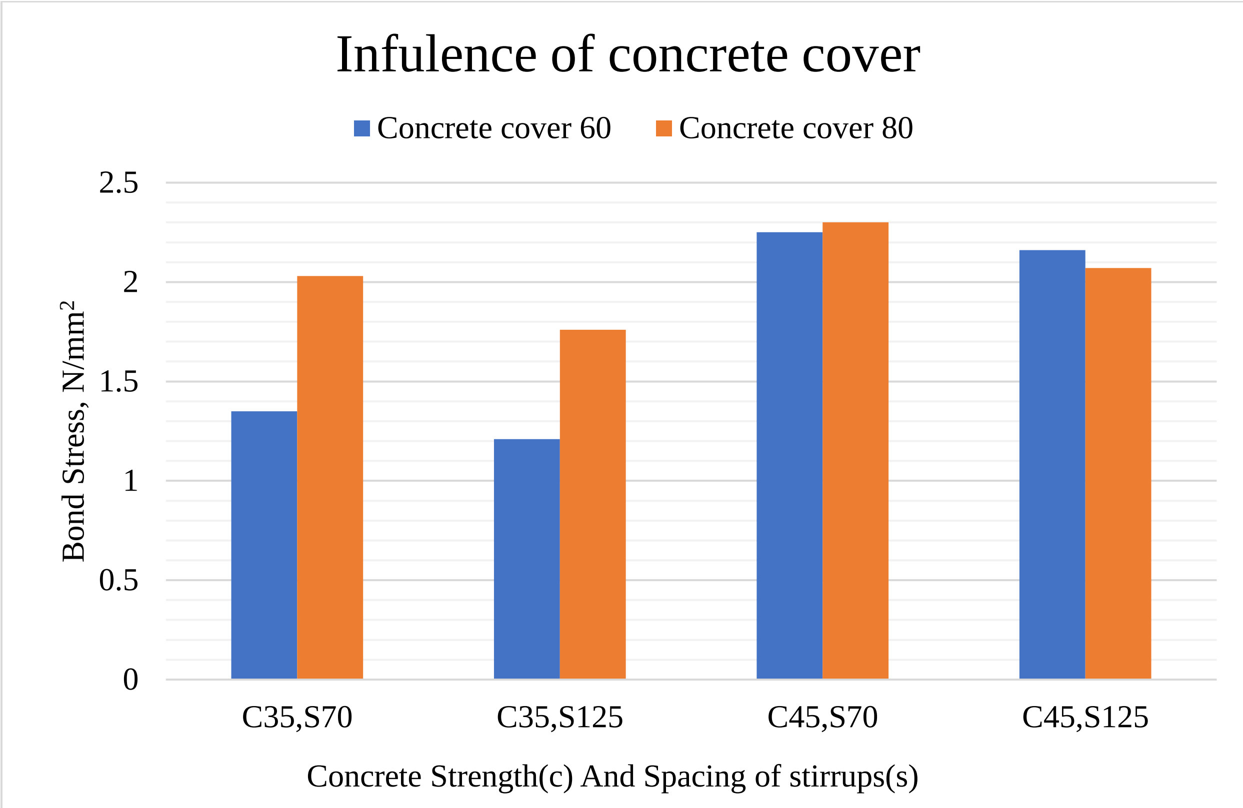

Fig 5. 20 Effect of Concrete cover

5.4.3 Spacing of Transverse Reinforcement

Lateral confinement of transverse reinforcement has no major effect on the maximum average bond stress. Lateral confinement is effective for fire exposed specimens on post slip performance (Tao and Yu, 2012 & Roeder, Chmielowski, *et al.*, 1999). The maximum average bond stress of CE-CFST 11, CE-CFST 13, CE-CFST 21, and CE-CFST 23 compared to that of CE-CFST 12 was 4%, CE-CFST 14 was 10%, CE-CFST 22 was 12.6%, and CE-CFST 24 was 13.3%, respectively, greater, shown in Fig 5.21.

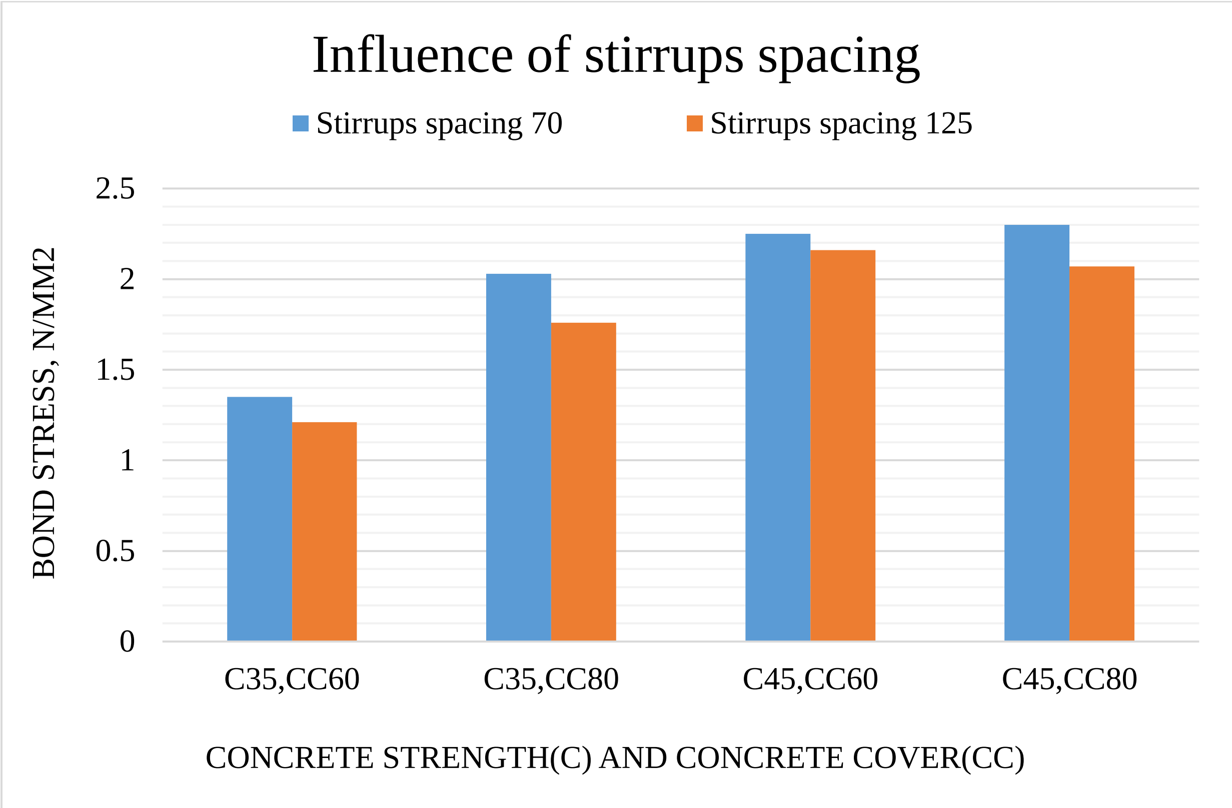

Fig 5. 21 Effect of lateral confinement

CHAPTER 6. VALIDATION OF FE MODEL

6.1 Bond Stress-Slip Curve

The load-slip curve obtained from the finite element analysis compared with the experimental results in Fig 6.1. The ultimate bond stress and ultimate slip of bond stress-slip relationship of experimental result have good agreement with the numerical analysis. A maximum of 9% and a minimum of 0.2% error are obtained in the ultimate bond stress and ultimate slippage for the experimental result and numerical results shown in Table 6.1. The mean and standard deviation ratio of ultimate bond strength of experimental to FEA was 0.980 and 0.061, respectively. Hence, the bond stress-slip relationship of outer concrete to the steel interfaces was successfully predicted by the non-linear finite element model.

Table 6. 1 comparison between experimental result to FE result

Specimen	Maximum push load, kN		
	Exp	FEM	Exp/FEM
CE-CFST11	277.11	260.601	1.063
CE-CFST12	288.89	266.14	1.085
CE-CFST13	265.11	288.597	0.921
CE-CFST14	294.37	303.37	0.972
CE-CFST21	156.31	162.2	0.964
CE-CFST22	172.57	189.89	0.91
CE-CFST23	225.51	241.67	0.943
CE-CFST24	260.1	260.47	0.998

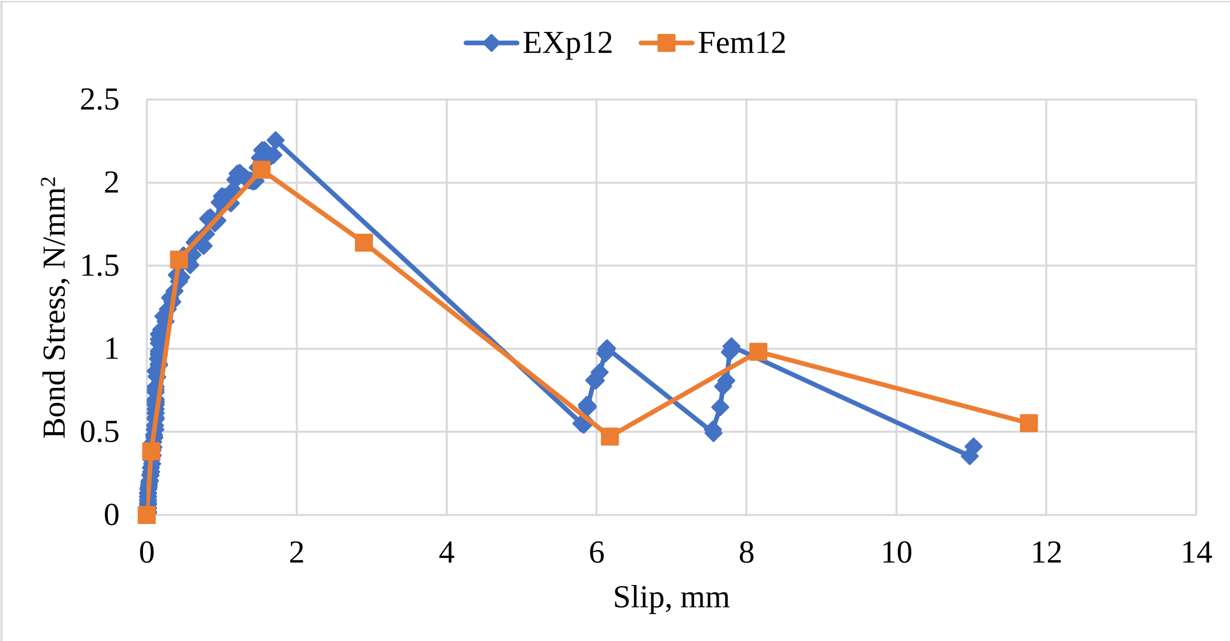

a. Comparison between FEM and Experimental result for CE-CFST12

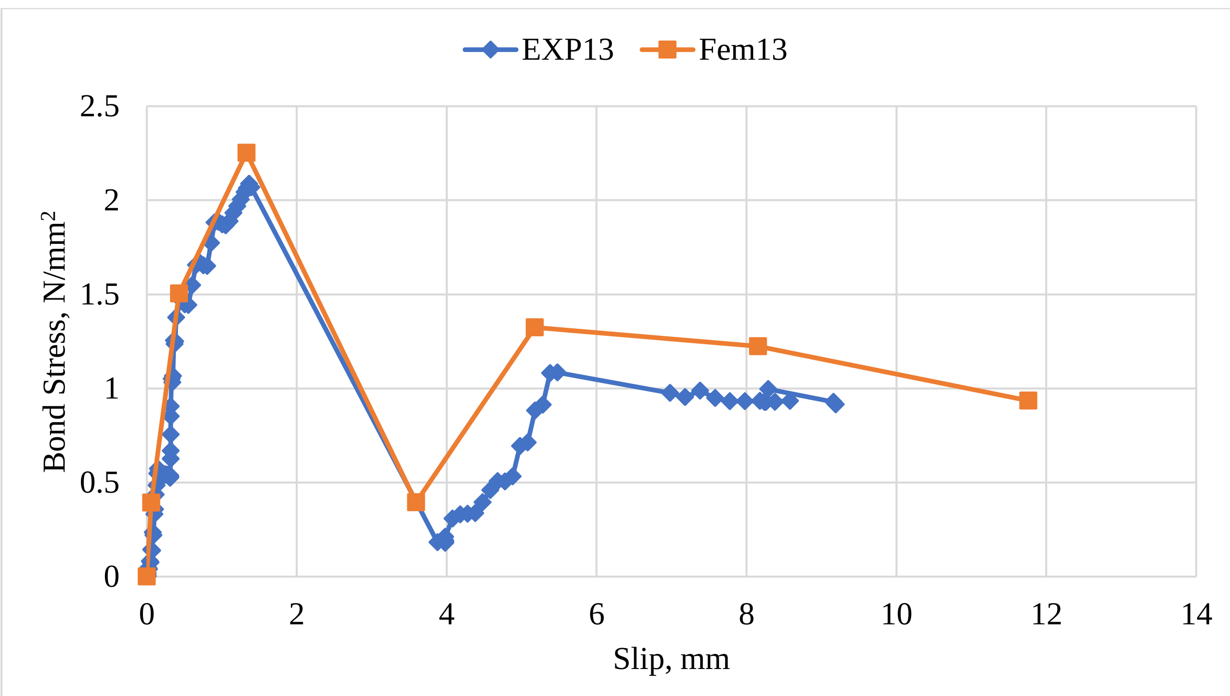

b. Comparison between FEM and Experimental result for CE-CFST13

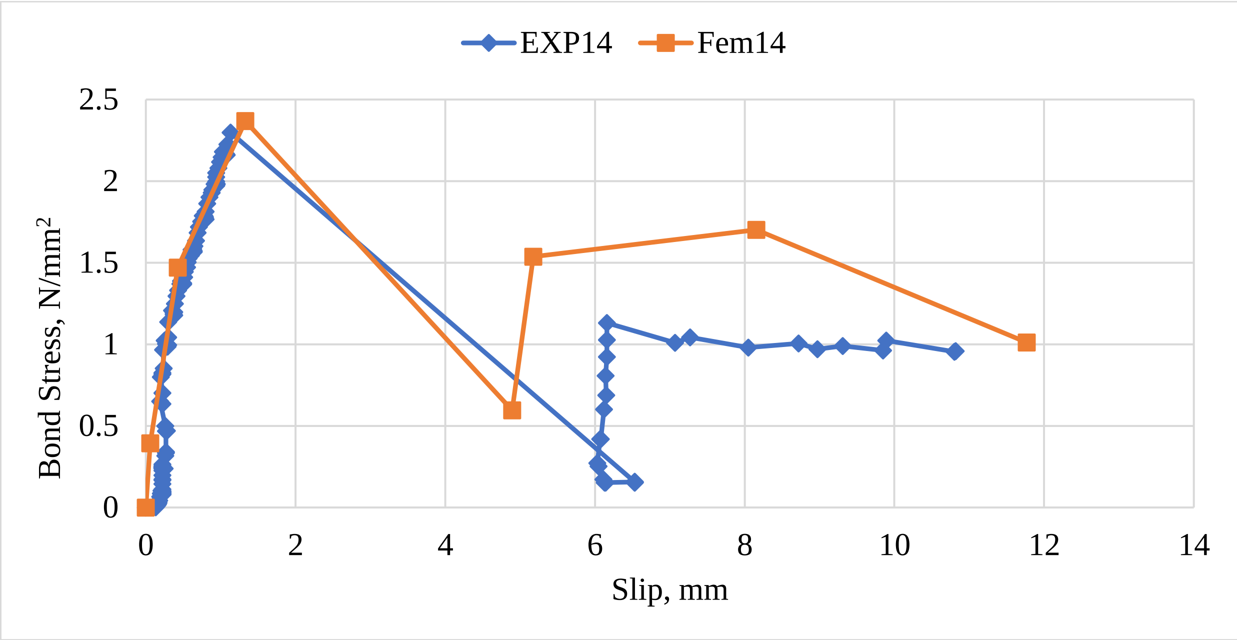

c. Comparison between FEM and Experimental result for CE-CFST14

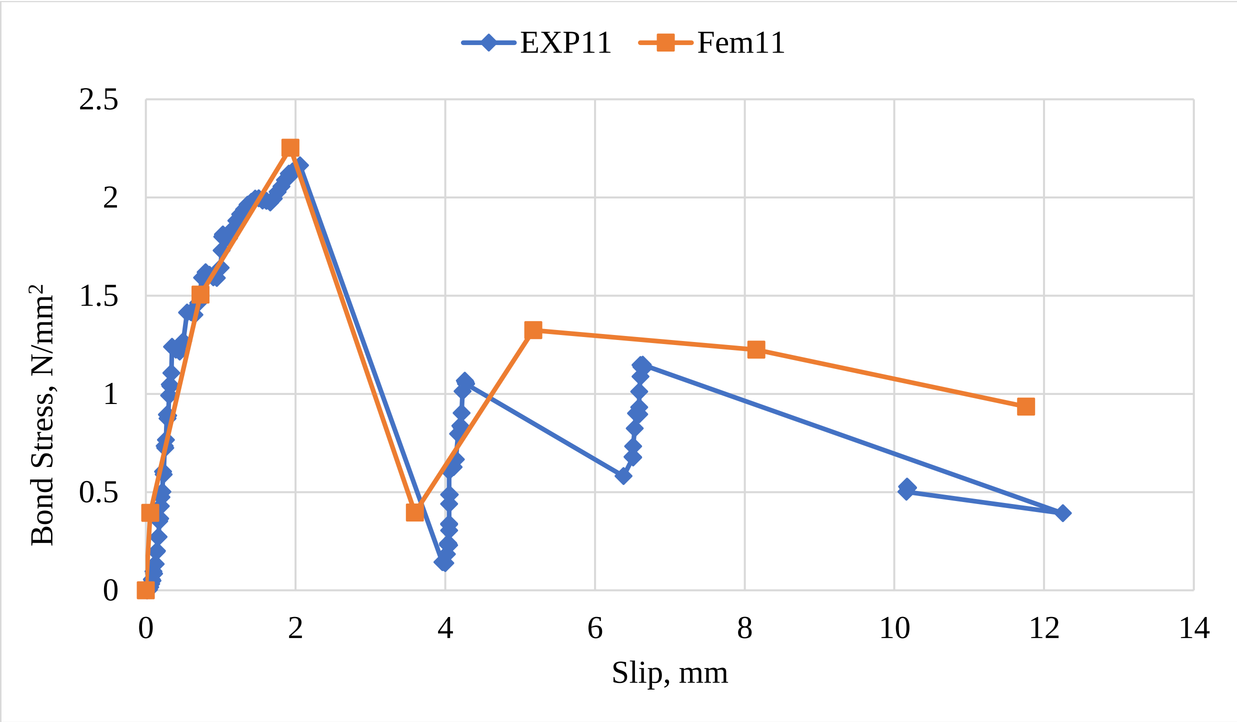

d. Comparison between FEM and Experimental result for CE-CFST11

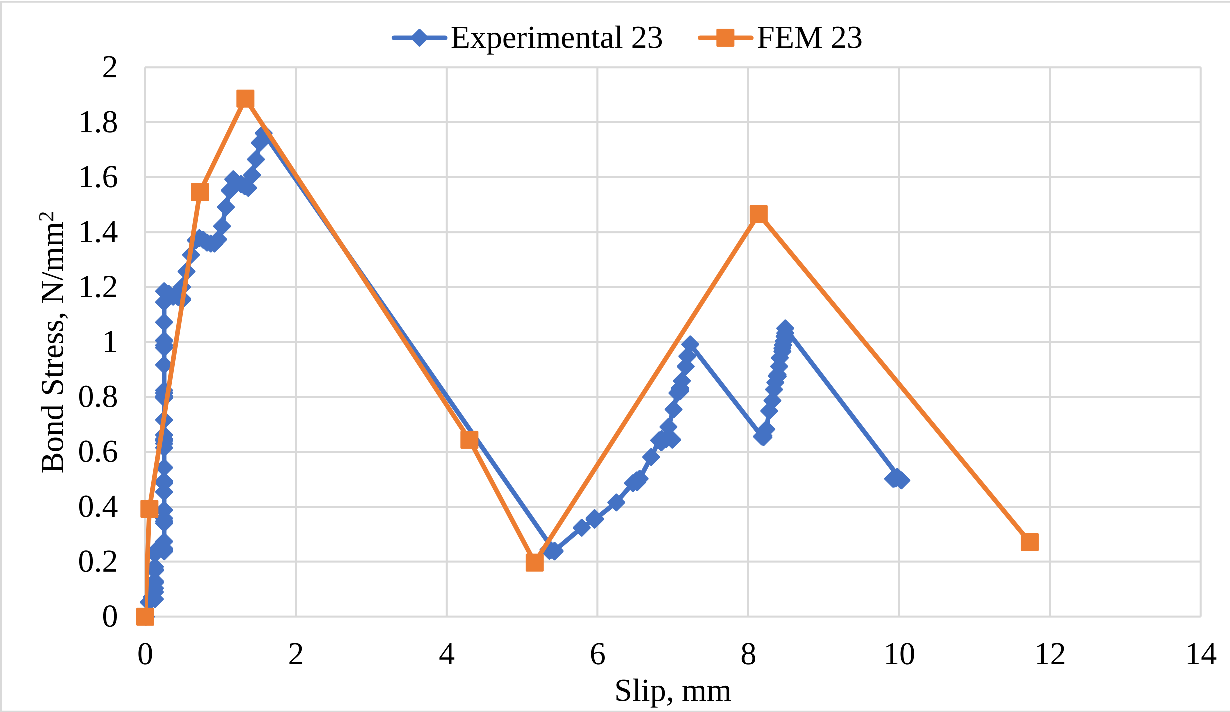

a. Comparison between FEM and Experimental result for CE-CFST23

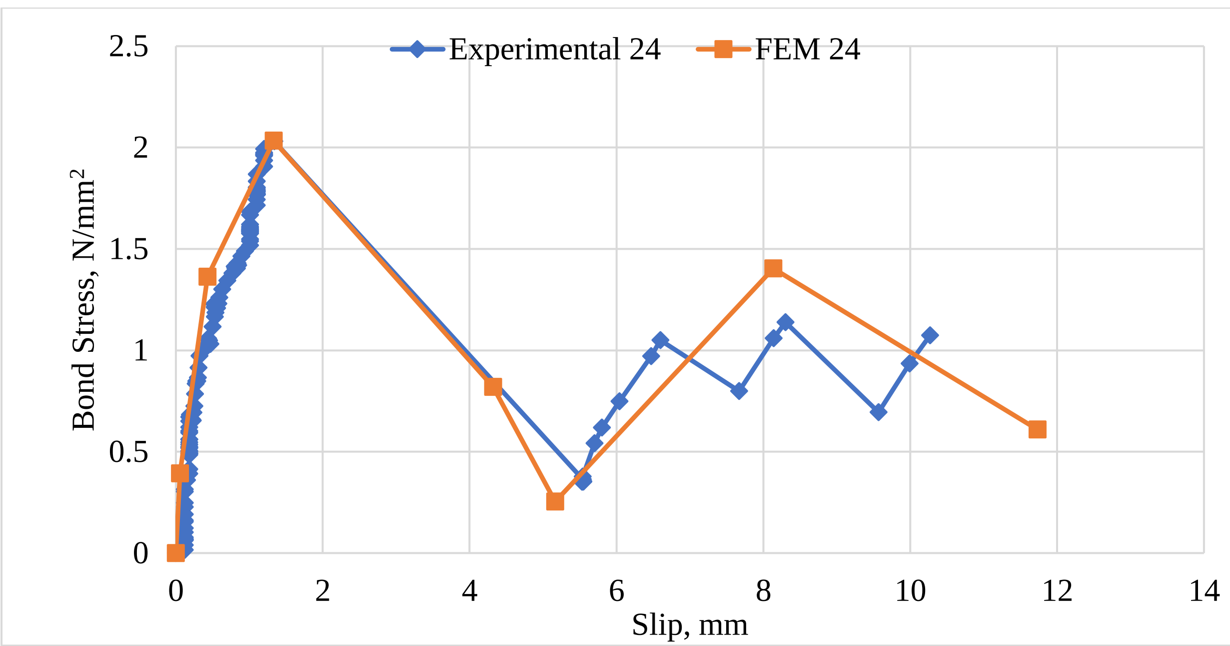

b. Comparison between FEM and Experimental result for CE-CFST24

Fig 6. 1 Validation of experimental result to FEM result

6.2 Failure Modes

The failure mode of concrete and steel from the experimental results are compared with the numerical analysis in Fig 6.2. The finite element analysis failure modes are successfully agreed with the pushout failure modes of concrete at the steel-concrete interfaces. The damage value of 0.7435 indicates the cracking of concrete in the finite element model, which designates that the finite element model accurately predicts the failure mode.

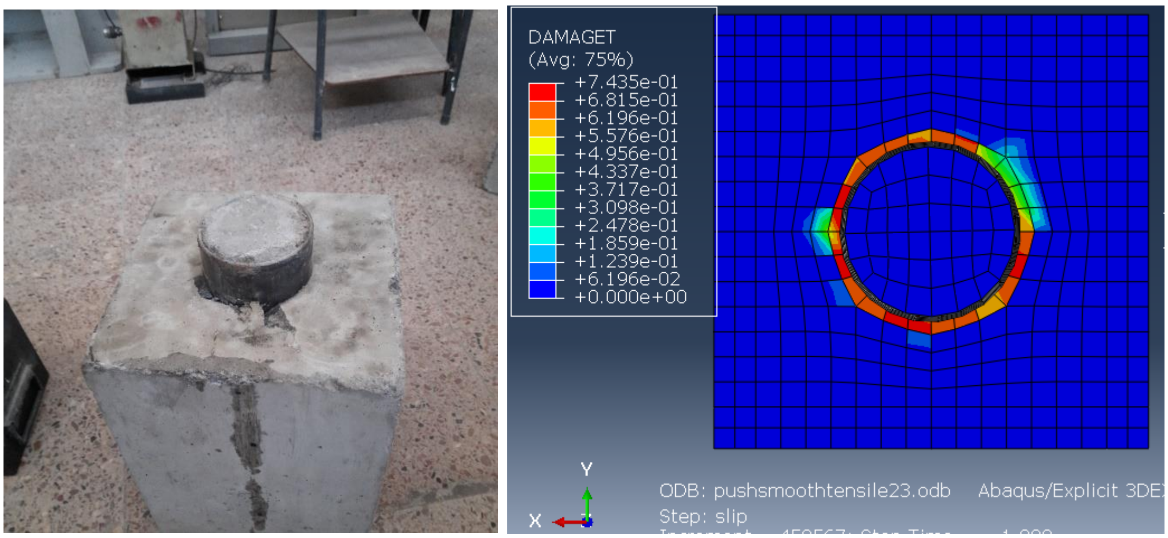

Fig 6. 2 Failure mode of concrete

6.3 Failure Process of Bonded Layer

Fig 6.3 provides the numerical results of the failure of cohesive surface, in which CSDMG represents the scalar stiffness degradation for the bonded surface. The value of CSDMG varies from 0 to 1. 0 means that no damage occurred, and 1 means that the bond at the interfaces entirely damaged. The damage of bonded surface measured at the half of the ultimate load, at the ultimate load, and the residual load. At the half of ultimate load, there is insignificant damage initiation was observed shown in Fig 6.3A. Further load increases produce interfacial damage at the interfaces, which propagates from the loaded end to the free end. At the ultimate load, the bonded surface excessively deteriorates at the interfaces of the steel tube, which the damage factor D is 0.9 shown in Fig 6.3B. At the residual load, the bonded surface was completely damaged with the damage factor of 1 shown in Fig 6.3C. The damage process of the bonded surface is well agreed with the failure of concrete at the interfaces and the friction marks of the steel tube to resist the slip.

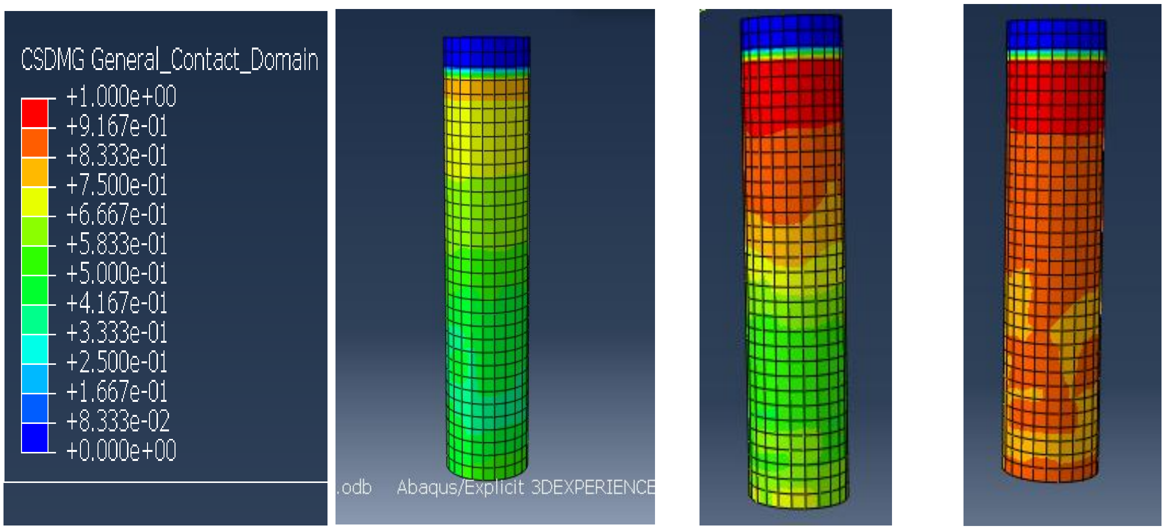

A, 50% *of peak load* B, *at the peak load* C, 60% *post peak load*

Fig 6. 3 Failure of bonded layer

Fig 6.4 show, the location of failure of bonded layer on the bond stress to slip curve. At point A (50% of peak load) there was no damage on the linear response. Then at point B, the initiation of damage at the peak bond stress to slip curve. At point C, there was damage evolution to full separation on the post softening region of the curve.

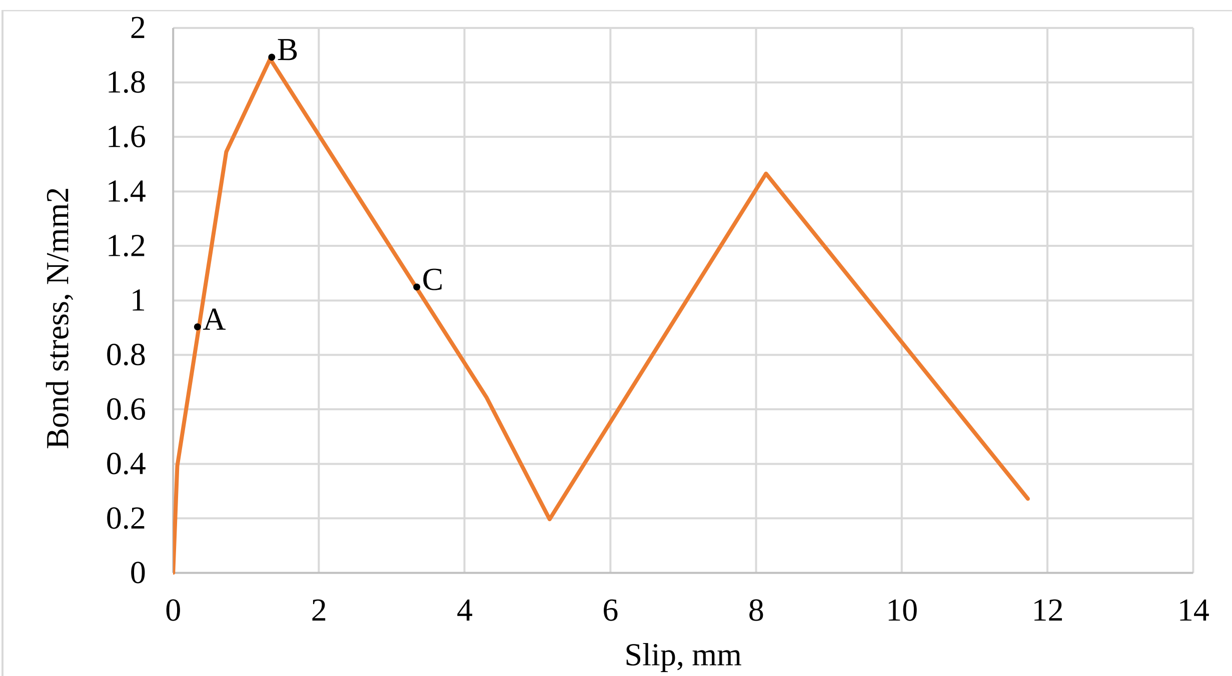

Fig 6. 4 Failure of bonded layer at the location of bond stress to slip curve

CHAPTER 7. CONCLUSION AND RECOMMENDATION

7.1 Conclusion

An experimental investigation to evaluate and assess the effect of various parameters on the natural bond performance between outer steel surface and outer reinforced concrete. Some conclusion can be made within the scope of the parameters studied as follows:

- The bond stress to slip curve shows four regions. The first region was a linear region, in which the bond resistance comes from chemical adhesion and micro interlock. As the slip increases, the non-linear stage will follow. In the second region, the chemical adhesion and micro interlock mainly contribute to shear transfer up to peak point. At the third post-peak softening stage, the bond stress decreases due to the loss of chemical adhesion. At the fourth residual stage, the chemical adhesion has vanished. And, reactivation of micro interlock and macro interlock contribute to the natural bond.
- The bond stress plays an important role in the load transfer between different components and load transferred from CFST to outer RC through bond stress, and strong bond strength was achieved between CFST and outer RC.
- The average bond strength of outer RC to CFST interfaces was 1.78N/mm^2, while the minimum and maximum bond strength were 1.18N/mm^2 and 2.3N/mm^2, respectively, which the bond strength values provided for shear stress limit in FEM.
- The bond strength increases with increases of concrete strength for 60mm concrete cover of CE-CFST specimen. But have a moderate effect on specimens with 80mm concrete cover.
- The bond strength increases with the increasing thickness of the concrete cover by. Nonetheless, for higher compressive strength, the effect of concrete cover on bond strength was insignificant which is 8.7% increases.
- The effect of lateral confinement is insignificant on the bond strength.
- The bond strength of each specimen satisfied the requirement of the Euro code 4 and ES EN1994:2015.

7.2 Recommendation

The following recommendation suggested for further investigation:

- ✓ A further experimental investigation should be conducted on the effect of concrete cover for high concrete strength on the bond performance.
- ✓ The effects of a shear connector or mechanical key on the bond strength need further investigation
- ✓ The strain distribution on the steel tube should be considered in future works.

REFERENCE

Abaqus Cae User's Manual (2012) 'Abaqus Cae User's Manual (6.12)', *Manuals*, P. 1174.

Aly, T. *Et Al.* (2010) 'Incremental Collapse Threshold For Pushout Resistance Of Circular Concrete Filled Steel Tubular Columns', *Journal Of Constructional Steel Research*. Elsevier Ltd, 66(1), Pp. 11–18. Doi: 10.1016/J.Jcsr.2009.08.002.

An, Y., Han, L. And Zhao, X. (2013) 'Finite Element Analysis On Concrete-Encased Cfst Stub Columns', 1, Pp. 2598–2608.

Birtel, V., Mark, P. And Bochum, R. (2006) 'Parameterised F Inite E Lement M Odelling Of Rc B Eam S Hear F Ailure', Pp. 95–108.

Ebcs-En1994:2013: (2013) 'Design Of Composite Steel And Concrete Structures', *Ababa, Addis*, (August).

Eurocode 4.1 (2004) 'Eurocode 4 : Design Of Composite Steel And Concrete Structures Part 1-1 : General Rules And Rules For Buildings', Pp. 1–117.

Feng, R. *Et Al.* (2018) 'Push-Out Tests Of Concrete-Filled Stainless Steel Shs Tubes', *Journal Of Constructional Steel Research*. Elsevier Ltd, 145, Pp. 58–69. Doi: 10.1016/J.Jcsr.2018.02.016.

Han, L. *Et Al.* (2016) 'Behavior Of Concrete-Encased Cfst Members Under Axial Tension', *Journal Of Structural Engineering*, 142(2), Pp. 1–12. Doi: 10.1061/(Asce)St.1943-541x.0001422.

Han, L. H. And An, Y. F. (2014) 'Performance Of Concrete-Encased Cfst Stub Columns Under Axial Compression', *Journal Of Constructional Steel Research*. Elsevier Ltd, 93, Pp. 62–76. Doi: 10.1016/J.Jcsr.2013.10.019.

Han, L. H., Ma, D. Y. And Zhou, K. (2018) 'Concrete-Encased Cfst Structures : Behaviour And Application', (Asccs), Pp. 1–10.

Han, L. H., Yao, G. H. And Tao, Z. (2007) 'Performance Of Concrete-Filled Thin-Walled Steel Tubes Under Pure Torsion', *Thin-Walled Structures*, 45(1), Pp. 24–36. Doi: 10.1016/J.Tws.2007.01.008.

Hoshikuma, B. J. *Et Al.* (1997) 'Stress-Strain Model For Confined Reinforced Concrete In Bridge Piers', *Journal Of Structural Engineering*, (1992), Pp. 624–633.

Jan A. Wium And Jean-Paul Lebet (1994) 'Simplified Calculation Method For Force', *Journal Of Structural Engieering*, 120(3), Pp. 728–746.

K.S. Virdi And P.J. Dowling (1980) 'Bond Strength In Concrete Filled Steel Tubes', *International Assocation For Bridge And Structural Engineering*, P-33/80, Pp. 125–139.

Khodaie, N. (2013) 'Effect Of The Concrete Strength On The Concrete-Steel Bond In Concrete Filled Steel Tubes', *Journal Of The Persian Gulf*, 4(11), Pp. 9–15.

Lee, Y. H. *Et Al.* (2011) 'Mechanical Properties Of Constitutive Parameters In Steel-Concrete Interface', *Engineering Structures*. Elsevier Ltd, 33(4), Pp. 1277–1290. Doi: 10.1016/J.Engstruct.2011.01.005.

Li, S., Han, L. H. And Hou, C. (2018) 'Concrete-Encased Cfst Columns Under Combined Compression And Torsion: Analytical Behaviour', *Journal Of Constructional Steel Research*. Elsevier Ltd, 144, Pp. 236–252. Doi: 10.1016/J.Jcsr.2018.01.020.

Li, W. *Et Al.* (2020) 'Experimental Study On The Performance Of Steel-Concrete Interfaces In Circular Concrete-Filled Double Skin Steel Tube', *Thin-Walled Structures*. Elsevier Ltd, 149(January), P. 106660. Doi: 10.1016/J.Tws.2020.106660.

Popovics, S. (1973) 'A Numerical Approach To The Complete Stress-Strain Curve Of Concrete', *Cement And Concrete Research*, 21(July), Pp. 1154–1157.

Qu, X. *Et Al.* (2013) 'Load-Reversed Push-Out Tests On Rectangular Cfst Columns', *Journal Of Constructional Steel Research*. Elsevier B.V., 81, Pp. 35–43. Doi: 10.1016/J.Jcsr.2012.11.003.

Qu, X. *Et Al.* (2015) 'Push-Out Tests And Bond Strength Of Rectangular Cfst Columns', *Steel And Composite Structures*, 19, Pp. 1–19.

Ren, Q. X. *Et Al.* (2017) 'Concrete-Encased Cfst Columns Under Combined Compression And Torsion: Experimental Investigation', *Journal Of Constructional Steel Research*. Elsevier Ltd, 138, Pp. 729–741. Doi: 10.1016/J.Jcsr.2017.08.016.

Roeder, B. C. W., Cameron, B., *Et Al.* (1999) 'Composite Action In Concrete Filled Tubes', 125(May), Pp. 477–484.

Roeder, B. C. W., Chmielowski, R., *Et Al.* (1999) 'Shear Connector Requirement For Embedded

Steel Section', 125(February), Pp. 142–151.

Tao, Z. *Et Al.* (2011) 'Post-Fire Bond Between The Steel Tube And Concrete In Concrete-Filled Steel Tubular Columns', *Journal Of Constructional Steel Research*. Elsevier Ltd, 67(3), Pp. 484–496. Doi: 10.1016/J.Jcsr.2010.09.006.

Tao, Z. And Yu, Q. (2012) 'Residual Bond Strength In Steel Reinforced Concrete Columns After Fire Exposure', *Fire Safety Journal*. Elsevier, 53, Pp. 19–27. Doi: 10.1016/J.Firesaf.2012.06.010.

Wang, X. *Et Al.* (2019) 'Effect Of Concrete Cover On The Bond-Slip Behavior Between Steel Section And Concrete In Src Structures', *Construction And Building Materials*. Elsevier Ltd, 229, P. 116855. Doi: 10.1016/J.Conbuildmat.2019.116855.

APPENDIX A

The following steps are used to model the CECFST by FEM(Abaqus):

1. Part module

The first step in fem is to define the part of the material. The cross-sectional size of CE-CFST is 220*220mm and 260*260mm, with a height of 460mm.

2. Property module

In this stage, material property and section are defined to the part. The CE-CFST is made up of concrete, steel tube, reinforcement, and plates. Thickness is assigned to the steel section at this stage.

3. Assembly module

In this stage, each part of CE-CFST member arranged to the exact position. Parts can be duplicated, rotated, and delated to represent the experimental results.

4. Step module

The step module provides an easy way to capture change for model loading and boundary parameter. It provides Adjustments in model loading and boundary conditions changes of how parts of the configuration communicate with each other, the elimination or inclusion of components, and any other modifications that may occur in the process during the analysis.

5. Interaction module

In the interaction stage, the interaction between different parts is selected such as concrete to steel, bars to concrete, CE-CFST to the rigid plate, CFST to load plate.

6. Load module

In finite element modeling, the load module is used for assigning the boundary conditions. The boundary condition is assigned Mechanical – Displacement/Rotation type to be the type of step. Apply the boundary condition U1, U2, U3, UR1, UR2, UR3. The load type is specified displacement in the U2 direction.

7. Mesh module

The development of a clean, uniform mesh for structural analysis was facilitated by improved meshing algorithms and software. The focus of this post is on the use of toolsets to improve mesh quality in partition or divide. Balanced mesh is used to avoid stress concentration on unwanted areas.

8. Job module

Nine CE-CFST columns under push load were analyzed using Abaqus finite element codes, these 9 CECFST are divided into three categories (concrete strength, concrete cover, and spacing of transverse reinforcement). The FEA successfully according to the prompt in the job monitor log file, the output data, and the result displayed in the visualization manual.